Inter-comparison of cosmogenic in-situ 3He, 21Ne and 36Cl at low latitude along an altitude transect on the SE slope of Kilimanjaro volcano (3°S, Tanzania)

Irene Schimmelpfennig, Alice Williams, Raphael Pik, Pete Burnard, Samuel Niedermann, Robert Finkel, Björn Schneider, Lucilla Benedetti

Inter-comparison of cosmogenic in-situ ^{3}He, ^{21}Ne and ^{36}Cl at low latitude along an altitude transect on the SE slope of Kilimanjaro volcano (3°S, Tanzania)

Irene Schimmelpfennig[a,b*], Alice Williams[a], Raphaël Pik[a], Pete Burnard[a], Samuel Niedermann[c], Robert Finkel[b,d], Björn Schneider[c], Lucilla Benedetti[b]

[a] CRPG, UPR 2300 CNRS, Nancy Universités, 15 rue Notre Dame des Pauvres, 54501 Vandoeuvre-lès-Nancy, France

[b] CEREGE, UMR 6635 CNRS, Université Paul Cézanne, Europôle de l'Arbois, 13545 Aix en Provence, France

[c] Helmholtz-Zentrum Potsdam – Deutsches GeoForschungsZentrum GFZ, Telegrafenberg, 14473 Potsdam, Germany

[d] Earth and Planetary Science Department, University of California Berkeley, Berkeley, CA 94720-4767, USA

[e] Vrije Universiteit, Department of Isotope Geochemistry, de Boelelaan 1085, 1081 HV Amsterdam, The Netherlands

* corresponding author. Present address: LDEO, Columbia University, Route 9W, Palisades, NY 10964, USA; Tel.: ++1 845 365 8653; Fax: ++1 845 365 8155; E-mail: schimmel@ldeo.columbia.edu

Abstract

Because the intensity and energy spectrum of the cosmic ray flux are affected by atmospheric depth and geomagnetic-field strength, cosmogenic nuclide production rates increase considerably with altitude and to a lesser degree with latitude. The scaling methods used to account for spatial variability in production rates assume that all cosmogenic nuclides have the same altitude dependence. In this study we evaluate whether the production rates of cosmogenic ^{36}Cl, ^{3}He and ^{21}Ne change differently with altitude, which is plausible due to the different threshold energies of their production reactions. If so, nuclide-specific scaling factors would be required.

Concentrations of the three cosmogenic nuclides were determined in mafic phenocrysts over an altitude transect between 1000 and 4300 m at Kilimanjaro volcano (3° S). Altitude-dependence of relative production rates was assessed in two ways: by determination of concentration ratios and by calculation of apparent exposure age ratios for all nuclide pairs. The latter accounts for characteristics of ^{36}Cl that the stable nuclides ^{3}He and ^{21}Ne do not possess (radioactive decay, high sensitivity to mineral composition and significant contributions from production reactions other than spallation). All ratios overlap within error over the entire transect, and altitudinal variation in relative production rates is not therefore evident. This suggests that nuclide-specific scaling factors are not required for the studied nuclides at this low latitude location. However, because previous studies have documented anomalous altitude-dependent variations in ^{3}He production at mid-latitude sites, the effect of latitude on cross-calibrations should be further evaluated.

We determined cosmogenic ^{21}Ne/^{3}He concentration ratios of 0.1864 ± 0.0085 in pyroxenes and 0.377 ± 0.018 in olivines, agreeing with those reported in previous studies.

Despite the absence of independently determined ages for the studied lava surfaces, the consistency in the data-set should enable progress to be made in the determination of the production rates of all three nuclides as soon as the production rate of one of the nuclides has been accurately defined.

To our knowledge this is the first time that ^{36}Cl has been measured in pyroxene. The Cl extraction method was validated by measuring ^{36}Cl in co-existing plagioclase phenocrysts in one of the samples.

Key words: Cosmogenic nuclides; Chlorine-36, Helium-3, Neon-21; Cross-calibration; Pyroxene; Olivine; Kilimanjaro; Altitude dependent scaling

1. Introduction

Accurate application of the surface-exposure dating technique, using terrestrial cosmogenic nuclides (TCN) such as ^{36}Cl, ^{3}He, ^{21}Ne, ^{10}Be or ^{26}Al, requires precise and accurate knowledge of the production rate of the nuclide of interest (the number of atoms produced per gram of target material per year) and the variation of this production rate in space and time (scaling). Reference production rates have been determined to allow application of the TCN method anywhere on Earth (see review in Gosse and Phillips, 2001). These are extrapolated to a particular location using scaling factors calculated according to one of the published scaling models (e.g. Stone, 2000, Dunai, 2001a, Desilets and Zreda, 2003, Lifton et al., 2005). Experimental calibrations of reference production rates are made by (1) measuring the concentration of the nuclide of interest in a geological sample from an independently dated surface at a specific geographic location, and (2) scaling the calculated time-integrated local production rate to the traditional reference position at sea-level and high latitude (SLHL) and to the present (Gosse and Phillips, 2001).

It is clearly imperative that scaling methods accurately quantify the spatial and temporal variability of TCN production on Earth. Recently however, some authors have cast doubt on our understanding of this variability, suggesting it could be one of the main causes for inconsistencies between calibrated SLHL production rates, thereby constituting a major source of uncertainty in TCN exposure ages (Balco et al., 2008, 2009, Schimmelpfennig et al., 2011).

Published scaling methods generally assume that the scaling factor for a particular type of nuclear-reaction (neutron- or muon-induced) is valid for all TCN and independent of the target element on which the reaction occurs. For example, at any given location production of ^{10}Be by spallation of Si and O is scaled using the same factor as production of ^{36}Cl by spallation

93 of Ca. However, this approach is controversial and the need for nuclide specific scaling
94 factors, as first discussed by Dunai (2001b), is currently being debated. The argument is based
95 on two aspects of TCN production. First, excitation functions for the various TCN production
96 reactions are known to be different (e.g. Desilets et al., 2006, Amidon et al., 2008 and
97 references therein). This means that the threshold energies (minimum energies of secondary
98 nucleons required for the reactions) and cross sections (probabilities of the occurrence of the
99 reaction at a certain nucleon energy) differ between the various production reactions. Second,
100 it has been hypothesized that the energy spectrum of the secondary nucleons shifts towards
101 lower energies with increasing atmospheric depth (Desilets and Zreda, 2003). For example,
102 the threshold energy for the production of ^{36}Cl from spallation of K (about 5 MeV) is lower
103 than that from spallation of Ca (about 20 MeV; see excitation functions in Fig. 2 in Desilets et
104 al., 2006). It might therefore be expected that the ratio of ^{36}Cl production from K to that from
105 Ca will increase with increasing atmospheric depth (i.e. decreasing altitude). If so, nuclide-
106 and even target-element-specific scaling factors would be needed.
107 One way of assessing TCN production and the global consistency in scaling is to determine
108 relative production rates of different TCN in geomorphic surfaces. These *cross-calibrations*
109 do not necessarily require that surfaces be independently dated nor perfectly preserved.
110 Measurements of multiple TCN in the same or in different mineral phases from a single
111 sample can be used to refine poorly known SLHL production rates using TCN with well-
112 constrained production rates (e.g. Amidon et al., 2009, Balco and Shuster, 2009, Goethals et
113 al., 2009). In addition, performing cross-calibrations over a range of altitudes, latitudes or
114 exposure times enables assessment of any spatial and/or temporal dependence in the
115 production of the different TCN. For example, Gayer et al. (2004) measured ^{3}He/^{10}Be in
116 Himalayan garnets over an altitude transect between 3000 and 4600 m and determined
117 production ratios higher than previously documented (Cerling and Craig, 1994). The apparent

^{3}He overproduction, which seemed to be prevalent at high altitude, was tentatively attributed to a significant difference in the threshold energies for the production of the two nuclides. More recently, Dunai et al. (2007) considered a second cosmogenic ^{3}He production mechanism, via low-energy neutron capture on ^{6}Li, to explain the higher ^{3}He production reported in Gayer et al. (2004). Some later studies were unable to identify an altitude-dependence unique to ^{3}He production (Blard et al., 2006, Vermeesch et al., 2009). In others, higher than expected apparent ^{3}He production rates were also inferred: at high altitudes in the Himalayas (Amidon et al., 2008) and on the Puna plateau in Argentina (Niedermann et al., 2009), and even at lower altitudes in the Coso Volcanic field and the Bishop Tuff (both in California, USA; Amidon et al., 2009, Niedermann et al., 2009).

In this study, we evaluate whether relative production rates of TCN change with altitude at a low-latitude site (3°S) and if overproduction of ^{3}He at high altitudes occurs. We cross-calibrate production of ^{3}He, ^{21}Ne and ^{36}Cl in lava-flow and glacial surfaces outcropping over an altitude profile between 1000 and 4300 m, on the slopes of Mt. Kilimanjaro, Tanzania. All three nuclides can be measured in clinopyroxene phenocrysts and this mineral phase provides the most complete data set in this study. In addition, ^{3}He was measured in olivine phenocrysts in all samples except one, and ^{21}Ne was measured in olivines at two different altitudes. To our knowledge, this is the first time that ^{36}Cl has been measured in a mafic mineral phase. To validate the method, ^{36}Cl was measured in plagioclase phenocrysts coexisting with pyroxenes in one of the samples.

2. Geological setting and sampling

Based on an initial project objective of calibrating absolute and relative production rates of TCN at a low-latitude site and over a large altitude transect, sampling was undertaken in 2005 at Mount Kilimanjaro, Tanzania (3°S) (Fig. 1). This large shield volcano, Africa's highest mountain (5892 m), is located at the eastern end of the Ngorongoro-Kilimanjaro Volcanic Belt, which forms one arm of the triple rift-system that characterizes the eastern branch of the East African Rift System. Kilimanjaro consists of three NW-SE aligned volcanic peaks, Shira (3962 m), Kibo (5892 m) and Mawenzi (5149 m), constructed in multiple phases. The first phase took place between 2.5 Ma and 1.9 Ma at the Shira vent (Nonnotte et al., 2008). A large sector collapse signalled the end of this phase, after which volcanic activity shifted eastwards to the Kibo and Mawenzi peaks, at around 1 Ma. Activity at Mawenzi ceased around 500 ka, but continued at Kibo with two major periods of volcanic activity occurring between 460 ka and 340 ka. The final stages of volcanism at Kilimanjaro consisted of the eruption of basaltic flows and scoria from small parasitic cones located on the volcano flanks, between around 200 ka and 150 ka (Nonnotte et al., 2008).

For this study, we principally targeted cones and lava flows from this last volcanic period in a region known as the Rombo Zone, located on the south-eastern flank, south of Mawenzi Peak (Downie and Wilkinson, 1972). This zone comprises olivine- and pyroxene-rich basanitic and ankaramitic flows erupted from parasitic cones distributed over a large elevation range, from < 1500 to > 4500 m. Suitable exposure of lava-flow surfaces is limited however between 1700 and 2500 m due to the presence of a dense tropical rainforest (Fig. 1). Flow-top preservation is also compromised above ~ 3700 m as a result of significant glacial activity during the Quaternary (Shanahan and Zreda, 2000).

While an effort was made to sample pristine flow-top features for absolute calibration of TCN production rates, at many sites this was not possible. Between 2700 and 3200 m, well-preserved ropy tops of lava-flows (Fig. A1 in Appendix) out-crop at the bases of parasitic cones. However, accessing the inner, degassed parts of the flow in order to extract rock suitable for precise Ar/Ar or K/Ar dating was difficult, and most flows were also too small and thin to have well developed massive interiors. As such, our efforts to obtain independent ages and absolute production rates for these flows were unsuccessful. For the parasitic cones erupted in the Rombo Zone, the only precise published eruption ages are K/Ar ages of 165 ± 5 ka and 195 ± 5 ka for two basaltic flows (Nonnotte et al., 2008), but their surfaces were not appropriate for exposure dating. For the investigation of relative TCN production rates, however, it is possible to use surfaces, such as glacially-polished surfaces, for which the eruption age of the lava-flow is not necessarily equal to the apparent exposure age.

Eight surface samples were collected at six different altitudes between 1000 and 4300 m (Table 1 and Fig. 1). Half of the samples were taken from well-preserved surfaces of two lava-flows (TZ10, TZ12, TZ13 and TZ14), two from eroding surfaces (TZ09, TZ17) and two from glacially polished surfaces (TZ15, TZ19). Based on field observations, the maximum rock thickness removed from the lava-flow at the lowest sample site at 1013 m altitude (TZ09) is estimated to be 30 cm. The surface of sample TZ17 also appeared to be slightly degraded in the field and the outcrop was surrounded by scoria and gravel deposits. Sample TZ15 was taken from a glacially polished doleritic dyke bearing large plagioclase laths in addition to pyroxene and minor olivine. A formation age of 527 ± 3 ka was determined for the dyke by $^{39}Ar/^{40}Ar$ dating (see Appendix). The exposure age of the surface can be expected to be significantly younger. The highest sample (TZ19) also exhibits slight glacial polishing. More detailed descriptions and photographs of sample sites are given in the Appendix.

- Fig. 1 about here -

- Table 1 about here -

3. Methods

3. 1 Physical sample preparation

Prior to sample preparation, pieces of whole rock from each surface were set-aside for thin-section preparation and bulk-rock composition analyses. For TCN analyses, the top 5 to 10 cm of each whole rock sample was sawn off, then crushed and wet-sieved to remove dust particles and the finest grain sizes (< 125 μm). A hand-magnet was passed over all fractions to remove magnetic groundmass. Using a binocular microscope, olivine and pyroxene phenocrysts were hand-picked to obtain pure mineral separates, with care taken to ensure complete removal of altered crystals and crystals with adhering groundmass. For ^{36}Cl analyses, approximately 5 to 10 g of pure pyroxene phenocrysts were handpicked from the coarsest fractions. For sample TZ15, a Frantz magnetic separator was used to separate several grams of 0.5-mm sized plagioclase phenocrysts from the more magnetic mafic minerals. Plagioclases were handpicked in order to maximize sample purity. For noble gas extractions, approximately 2 g of the coarsest pure fractions were cleaned in acetone and set aside for in vacuo crushing and determination of magmatic helium isotope ratios. For the melt extractions, up to 3 g of phenocrysts from the 0.5 to 0.7 mm size fraction were cleaned in acetone, hand-crushed and sieved to 0.1 - 0.3 mm and then re-picked and cleaned once more in acetone, to ensure the highest degree of sample purity.

213 **3. 2 Chemical ^{36}Cl extraction and measurement**

214 Chemical extraction of ^{36}Cl was conducted at CEREGE (Aix en Provence, France). The
215 procedure is detailed in the Appendix. Several procedural blanks were performed in order to
216 assess cleanliness during chemical extraction and to correct sample measurements for
217 laboratory ^{36}Cl and stable Cl sources.

218 Concentrations of ^{36}Cl and Cl were determined using the Lawrence Livermore National
219 Laboratory FN accelerator mass spectrometer (LLNL-CAMS, USA). Isotope dilution
220 (addition of a ^{35}Cl-enriched carrier) allows simultaneous determination of ^{36}Cl and Cl
221 concentrations. ^{36}Cl/^{35}Cl ratios were determined by normalizing to a ^{36}Cl standard prepared by
222 K. Nishiizumi (Sharma et al., 1990). The stable ratio ^{35}Cl/^{37}Cl was also normalized to this
223 standard, assuming a natural ratio of 3.127. Measured ratios and their uncertainties are
224 presented in Table A1 in the Appendix. The precision of the ^{35}Cl/^{37}Cl ratios accounts for 2% or
225 less (standard deviation of repeat measurements). The precision of the ^{36}Cl/^{35}Cl ratios ranges
226 from 2 to 7%.

227 Blank ^{36}Cl/^{35}Cl ratios range between 7×10^{-15} and 9×10^{-15}, and are one to two orders of
228 magnitude lower than the sample ^{36}Cl/^{35}Cl ratios (Table A1). The resulting blank-corrected ^{36}Cl
229 and Cl concentrations range from (0.63 to 5.25) $\times 10^{6}$ atoms ^{36}Cl g^{-1} and from 1 to 10 ppm Cl,
230 respectively (Table A1). The ^{36}Cl concentrations are also given in Table 3.

231

232 **3.3 Noble gas measurements**

233 Helium measurements were carried out using the Helix Split Flight Tube and Helix Multi-
234 collector mass spectrometers (GV instruments) at CRPG (Nancy, France) and a VG-5400
235 mass spectrometer at GFZ (Potsdam, Germany) (Table A3 in the Appendix shows where each
236 measurement was made). Neon measurements were performed with the VG-5400 mass
237 spectrometer at GFZ. While samples were degassed in a single step at CRPG, a two-step

238 heating procedure (900°C and 1750°C) was used at GFZ in order to separate a possible high
239 atmospheric Ne component from the major cosmogenic fraction. Mass spectrometers were
240 cross-calibrated by way of internal standard replication and measurement of CRONUS-EU
241 mineral standards. Further details of these inter-comparisons and of the noble gas extraction
242 and measurement procedures in the two laboratories can be found in the Appendix.
243
244 Determination of cosmogenic ^{3}He concentrations
245 Concentrations of cosmogenic ^{3}He in pyroxene and olivine are traditionally calculated from
246 melt and crush measurements using an equation that corrects for the trapped (magmatic) He
247 component (Kurz, 1986):
248
249 $$^{3}He_{cos} = {}^{3}He_{m} - {}^{4}He_{m} \times ({}^{3}He/{}^{4}He)_{mag} \qquad \text{Eq. 1}$$
250
251 where $^{3}He_{cos}$ is the cosmogenic ^{3}He concentration, $^{3}He_{m}$ and $^{4}He_{m}$ are the concentrations of ^{3}He
252 and ^{4}He measured from melt extractions and $(^{3}He/^{4}He)_{mag}$ is the magmatic ^{3}He/^{4}He value,
253 normally determined from phenocryst crush extractions. Because of insufficient sample
254 material and low He yields, not all $(^{3}He/^{4}He)_{mag}$ values in this study were determined by
255 crushing. Isochron intercepts according to the method by Blard and Pik (2008) were used for
256 samples TZ17 and TZ19 (Fig. A2 in Appendix). For samples TZ09 and TZ15 the value for
257 $(^{3}He/^{4}He)_{mag}$ was estimated. A description of the magmatic ^{3}He/^{4}He determinations is given in
258 the Appendix.
259 A critical step in the determination of cosmogenic ^{3}He is the correction for the implanted or
260 ingrown radiogenic ^{4}He (^{4}He*), which may be significant even in very young rocks (e.g. Dunai
261 and Wijbrans, 2000, Blard and Farley, 2008, Blard and Pik, 2008). In this study, for partially
262 eroded volcanic surfaces (TZ09 and TZ17) and glacially polished surfaces (TZ15 and TZ19),

263 $^{4}He^{*}$ was estimated from whole-rock and phenocryst U and Th concentrations following
264 Farley et al. (2006). The calculated $^{4}He^{*}$ was subtracted from the $^{4}He_{m}$ abundance prior to
265 using Eq. 1. For TZ09, TZ17 and TZ19, the magnitude of $^{4}He^{*}$ correction ranged between 4%
266 and 25% of total $^{4}He_{m}$; for pyroxene and olivine replicates of TZ15 it was calculated to be 53%
267 to 68% based on the rock formation age of ~525 ka (see discussion in section 4.2). For the
268 non-eroded volcanic surfaces (TZ10, 12, 13, 14) we applied the R-factor correction of Blard
269 and Pik (2008). The R-factor is a function of the production rate ratio between $^{4}He^{*}$ and $^{3}He_{cos}$,
270 which is constant over time for non-eroded volcanic surfaces, and $(^{3}He/^{4}He)_{mag}$. The R-factor
271 values for all four samples are > 0.98 (see Table A3 in the Appendix), which corresponds to a
272 $^{4}He^{*}$ correction of < 2%.
273 Helium data were systematically obtained for pyroxenes and olivines, except for sample TZ09
274 where only pyroxenes were available in sufficient quantity. Full raw data and calculated
275 cosmogenic ^{3}He concentrations are presented in Table A3. Concentrations of $^{3}He_{cos}$ range from
276 (9.6 to 99.8) × 10^{6} at g^{-1} in pyroxenes and from (13.1 to 97.9) × 10^{6} at g^{-1} in olivines.
277 Relative $^{3}He_{cos}$ production in the two minerals is compared in Fig. 2. As observed in previous
278 studies (e.g. Blard et al., 2005, Fenton et al., 2009), for most samples, cosmogenic ^{3}He
279 concentrations in cogenetic olivines and pyroxenes are identical within analytical uncertainty.
280 The exceptions are samples TZ13 and TZ10, where the concentrations in olivine are ~8%
281 lower than in pyroxene, and sample TZ15, where a difference of ~17% is observed. The latter
282 might be explained by an inaccurate magmatic He correction due to the high $^{4}He^{*}$ correction
283 estimated for this sample.
284 For those sites where two samples were taken from a single flow (TZ10 and TZ12 at 2740m;
285 TZ13 and TZ14 at 3050m) the $^{3}He_{cos}$ concentrations in pyroxenes differ by 10% (TZ10 and
286 TZ12) and 7% (TZ13 and TZ14) and in the olivines of TZ13 and TZ14 by 12%. The
287 concentrations in the olivines of TZ10 and TZ12 agree within analytical uncertainties (1σ).

288

289 - Fig. 2 about here -

290

291 Determination of cosmogenic ^{21}Ne concentrations

292 In young (< 500 ka) basalts concentrations of cosmogenic ^{21}Ne are calculated using:

293

294 $$^{21}Ne_{cos} = [(^{21}Ne/^{20}Ne)_m - (^{21}Ne/^{20}Ne)_{tr}] \times {}^{20}Ne_m \qquad \text{Eq. 2}$$

295

296 (Niedermann, 2002), where $^{21}Ne_{cos}$ is the cosmogenic ^{21}Ne concentration, $(^{21}Ne/^{20}Ne)_m$ and $^{20}Ne_m$
297 are the measured Ne isotope ratio and concentration from melt extractions, and $(^{21}Ne/^{20}Ne)_{tr}$ is
298 the trapped $^{21}Ne/^{20}Ne$ value. Most subaerially erupted basalts have a trapped Ne isotopic
299 composition similar to that of atmospheric Ne (e.g. Dunai and Porcelli, 2002, Althaus et al.,
300 2003), with isotope ratios of $^{21}Ne/^{20}Ne = 0.00296$ and $^{22}Ne/^{20}Ne = 0.1020$ (Eberhardt et al.,
301 1965). It is assumed in this calculation that the nucleogenic ^{21}Ne component is insignificant.
302 Neon isotope data are presented in Table A4 and in Fig. 3. All isotope data have been
303 corrected for isobaric interferences, mass discrimination effects and analytical blanks (see
304 Appendix). Examination of neon measurements on a three-isotope plot enables assessment of
305 the neon inventory in a sample. In Fig. 3, olivine and pyroxene data are defined by a linear
306 regression line $y = 1.0539x + 0.0994$, which is the same, within error, as the spallation line for
307 pyroxenes ($[1.069 \pm 0.035]x + 0.099$) reported by Schäfer et al. (1999). The regression line
308 passes through the air component and no nucleogenic or mantle component is identified in the
309 heating steps. This supports our assumption that the trapped component has an atmospheric
310 composition.
311 Concentrations of $^{21}Ne_{cos}$ range from (2.79 to 19.0) $\times 10^6$ at g^{-1} in pyroxenes and from (24.8 to
312 34.9) $\times 10^6$ at g^{-1} in olivines (Table 3). In the four samples containing cogenetic olivine and

pyroxene, $^{21}Ne_{cos}$(px)/$^{21}Ne_{cos}$(ol) range from 0.50 to 0.54. These are indistinguishable from the values predicted by modelling $^{21}Ne_{cos}$ production rates for the olivines (Fo_{81}) and pyroxenes (En_{41-43}) in this study ($^{21}Ne_{cos}$(px)/$^{21}Ne_{cos}$(ol) = 0.50 to 0.53) using major element compositions determined by microprobe and the elemental production rates of Masarik (2002) (see Table 2c). Our values are also the same within analytical error as (i) a measured ratio of 0.49 ± 0.07, deduced from the ^{21}Ne concentrations in cogenetic olivines (Fo_{82}) and pyroxenes (En_{44}) of sample 250406-16 in Fenton et al. (2009), and (ii) a calculated ratio of 0.56 ± 0.18, determined from experimentally calibrated ^{21}Ne production rate values for olivines and pyroxenes ($P^{21}Ne_{cos}(Fo_{81})$ = 45 ± 4 atoms g^{-1} a^{-1}, Poreda and Cerling, 1992; $P^{21}Ne_{cos}(En_{43-44})$ = 25 ± 8 atoms g^{-1} a^{-1}, Fenton et al., 2009). The large uncertainty associated with the experimental production rate ratio is mainly a function of the 32% uncertainty in the independent lava-flow age determined in the study of Fenton et al. (2009). Despite the differences in pyroxene composition among the samples and experimental production rates, our mean value of 0.52 ± 0.02 thus seems a reasonable estimate of the relative production ratio of ^{21}Ne in olivines (Fo_{81-82}) and pyroxenes (En_{41-44}).

Both olivine $^{21}Ne_{cos}$ concentrations and pyroxene $^{21}Ne_{cos}$ concentrations of samples TZ10 and TZ12 (flow at 2740 m) agree within analytical error (1σ). Also, for the samples taken from the flow at 3050 m (TZ13 and TZ14), the olivine $^{21}Ne_{cos}$ concentrations in the two samples are identical within uncertainties, but the concentration of $^{21}Ne_{cos}$ in the pyroxenes is 12% higher in TZ14 than in TZ13.

- Fig. 3 about here -

3.4 Major and trace elements

For the calculations of cosmogenic ^{36}Cl, chemical compositions of the mineral aliquots and of bulk-rock were analyzed at the Service d'Analyse des Roches et des Minéraux du CNRS (CRPG, Nancy, France). Major elements were determined by ICP-OES and trace elements by ICP-MS, except Li (atomic absorption), B (colorimetry), H_2O (Karl Fischer titration) and Cl (spectrophotometry). Bulk-rock concentrations of the major elements and of H, Li, B, Sm, Gd, U, Th and Cl are given in Table A2. These are required for calculating low-energy neutron distributions at the land/atmosphere interface. Aliquots of the etched mineral grains, taken before their complete dissolution, represent the part of sample dissolved for ^{36}Cl extraction and served for the analysis of the corresponding target element concentrations (Ca, K, Ti and Fe). These concentrations (Table 2a) and the Cl concentrations, determined by isotope dilution during AMS measurements (Table A1), were used to calculate ^{36}Cl production from all production mechanisms in the dissolved samples.

U and Th concentrations in groundmass and phenocryst separates, required for calculation of $^{4}He^*$ (as described in the previous section), were measured by ICP-MS at CRPG using the procedure optimized for low abundances in (U-Th)/He dating (Carignan et al., 2001; Kraml et al., 2006). Measured U and Th concentrations are listed in Table 2b (minerals) and Table A2 (groundmass). Li concentrations in the phenocrysts are required to estimate the cosmogenic ^{3}He production from thermal and epithermal neutron capture on ^{6}Li. The concentrations were measured at CRPG and are listed in Table 2b.

The compositions of chemically untreated olivine and pyroxene phenocrysts were determined by electron microprobe at l'Université Henri Poincaré, Nancy (Table 2c) and served to assess dependence of ^{21}Ne production on mineral composition (see previous section). Elemental production rates estimated for ^{21}Ne by Masarik (2002) are also given in Table 2c.

- Table 2 about here –

- Table 3 about here -

4. Approaches to TCN cross-calibrations

A common approach for comparing different TCN production rates in the same sample is to calculate ratios of cosmogenic nuclide concentrations. This approach has previously been adopted for cross-calibration of ^{3}He and/or ^{21}Ne production rates with ^{10}Be (Gayer et al., 2004, Kober et al., 2005, Farley et al., 2006, Amidon et al., 2008, Amidon et al., 2009), and for evaluation of relative ^{3}He and ^{21}Ne production rates (Fenton et al., 2009). When cross-calibrating TCN in several samples along an altitude transect, an increasing or decreasing trend versus altitude would indicate that the nuclides have different altitude dependences (Gayer et al., 2004, Amidon et al., 2008).

In these studies, the compared nuclides are primarily produced by spallation reactions. In the case of the noble gases ^{3}He and ^{21}Ne, trapped nucleogenic and radiogenic contributions were subtracted prior to cross-calibration, so that only cosmogenic components were taken into account. Predominantly spallation-produced nuclides such as ^{3}He, ^{21}Ne and ^{10}Be should accumulate in a given sample with a constant ratio. However, despite the fact that these nuclides are predominantly spallogenic in origin, there are nevertheless variations in production rate related to the chemical composition of the mineral involved.

1) Cosmogenic production of ^{3}He by thermal neutron capture on ^{6}Li has been shown to be potentially significant in Li-rich minerals and rocks (Dunai et al., 2007) and may require a correction. This approach has not been done in the pioneer paper of Gayer et al. (2004) but has since been addressed (e.g. Amidon et al., 2009). However, Li concentrations in mafic

386 minerals such as olivine and pyroxenes are generally low (< 10 ppm). In this study Li
387 concentrations range between 2 and 7 ppm (Table 2b) and thus contribute less than 1% to the
388 ^{3}He budget.
389 2) Even though ^{3}He and ^{21}Ne are commonly calibrated for a given mineral phase, their
390 production rates also depend on the mineral chemical composition (e.g. Masarik and Reedy,
391 1996). ^{3}He is mainly produced from O and Si, as well as from Mg, Fe, Al and Ca, with
392 relatively uniform elemental production rates. In contrast, ^{21}Ne is not produced from O, but
393 from Na, Mg, Al, Si, Ca and Fe with significant variations between elemental production rates
394 (e.g. Masarik and Reedy, 1996, Masarik, 2002, see Table 2c). The production rate of ^{21}Ne is
395 therefore more sensitive than that of ^{3}He to variations in mineral composition. As a
396 consequence, if the composition of a mineral phase varies significantly within the sample set,
397 ^{3}He/^{21}Ne ratios may also vary significantly.
398
399 While relative ^{3}He, ^{21}Ne and ^{10}Be production rates are only slightly dependent on mineral
400 chemistry, the situation is significantly more complex for ^{36}Cl. In order to compare spallogenic
401 nuclides with ^{36}Cl, three issues have to be considered.
402 i) Mineral composition is more important when comparing cosmogenic noble gas
403 concentrations to those of ^{36}Cl. ^{36}Cl is produced from fewer target elements than ^{3}He and ^{21}Ne,
404 dominantly from Ca, K and ^{35}Cl (review in Schimmelpfennig et al., 2009), making its
405 production rate extremely sensitive to the mineral composition.
406 ii) The noble gases ^{3}He and ^{21}Ne are stable TCN, while ^{10}Be and ^{36}Cl are radioactive.
407 Concentration ratios of a stable and a radioactive nuclide will not remain constant over long
408 exposure durations due to decay of the radionuclide. In the case of ^{10}Be, which has a half-life
409 of 1.39 Ma (Chmeleff et al., 2010, Korschinek et al., 2010), this becomes significant for
410 exposure ages longer than 100 ka, while in the case of the shorter-lived ^{36}Cl (half-life 301 ka),

411 the effect is significant for even shorter exposure durations. In addition, the effect depends on
412 erosion (Goethals et al., 2009), whereas the stable nuclides (^{3}He, ^{21}Ne) accumulate with a
413 constant ratio, irrespective of erosion rate. For example, the concentration ratio of ^{36}Cl/^{3}He or
414 ^{36}Cl/^{21}Ne is approximately 12% smaller than their production ratio for a 100 ka old surface
415 eroding at <1 m/Ma; at lower ages or higher erosion rates the difference becomes smaller
416 (according to Goethals et al., 2009; the muogenic ^{36}Cl contribution is neglected here).
417 Therefore, radioactive decay should be taken into account when comparing TCN
418 concentrations, especially if the samples have a range of exposure ages as they do in this
419 study.
420 iii) Cosmogenic ^{36}Cl is not only produced by spallation. A significant ^{36}Cl contribution is also
421 derived from slow negative-muon capture by Ca, and to a lesser degree by K (review in
422 Schimmelpfennig et al., 2009). Because the altitude-dependence of the muon flux is weaker
423 than that of the fast neutrons (e.g. Stone, 2000), with increasing altitude the production of ^{36}Cl
424 by spallation increases at a higher rate than ^{36}Cl production by muon-capture. Hence, over a
425 given altitude transect, total ^{36}Cl production will not be proportional to the production of TCN
426 derived almost purely from spallation. ^{36}Cl is also produced by thermal and epithermal neutron
427 capture on the trace element ^{35}Cl, and a significant proportion of ^{36}Cl can result from a high
428 level of Cl (>50 ppm) in a sample (Schimmelpfennig et al., 2009). However, as for ^{3}He
429 production due to ^{6}Li, when Cl concentrations in a sample are low (a few ppm) this
430 mechanism contributes generally insignificantly to the ^{36}Cl production. Variations in ^{36}Cl
431 concentrations in samples of the same lithology might therefore be a consequence of varying
432 Cl concentrations.
433
434

4.1 Comparing cosmogenic ^{36}Cl, ^{3}He and ^{21}Ne concentrations

Because of the favourable chemical composition of the pyroxene phenocrysts in our samples (notably low Cl, low K concentrations and similar Ca concentrations) we first directly compare the ratios of the cosmogenic ^{36}Cl, ^{3}He and ^{21}Ne concentrations (Fig. 4), ignoring the effects of radioactive decay, erosion and muogenic ^{36}Cl contribution. The ^{36}Cl contribution from Ca spallation is maximized by extraction from the Cl-poor, Ca-rich pyroxenes (max. 10 ppm Cl, see Table A1). Hence, spallation of Ca contributes between 86% and 90% of ^{36}Cl in these samples, while the contribution from spallation of K is < 1% and that from spallation of Ti and Fe together is about 3% (calculated using the ^{36}Cl calculation spreadsheet published in Schimmelpfennig et al., 2009). The contributions from thermal and epithermal neutron capture on ^{6}Li and ^{35}Cl, respectively, are < 1% for ^{3}He and 3.7% or less for ^{36}Cl. The Li-derived ^{3}He contribution is based on Li concentrations measured in the minerals, Table 2b, and calculated using a version of CHLOE (Phillips and Plummer, 1996) modified for ^{3}He production (R. Pik and P. Burnard, unpublished). The ^{36}Cl contributions due to slow negative-muon capture are 10% at 1000 m altitude and decrease to 5% at 4300 m. As a consequence we might expect a slight overestimate of the ^{36}Cl to noble gas nuclide ratios at low altitudes relative to high altitudes due to the muogenic ^{36}Cl contribution.

Since, to our knowledge, ^{36}Cl has never been measured in pyroxene before, we validate this method by measuring ^{36}Cl in co-genetic plagioclases in sample TZ15. Feldspar is an accepted ^{36}Cl target mineral (Stone et al., 1996, Evans et al. 1997, Schimmelpfennig et al. 2009). The ^{36}Cl concentrations in both mineral phases of TZ15 are given in Table A1 in the Appendix. Since the Ca concentrations are higher in the pyroxene by almost a factor of two and also the K and Cl concentrations differ between both mineral phases, ^{36}Cl concentrations cannot be directly compared. We therefore calculated the apparent exposure ages from these two minerals using the ^{36}Cl calculation spreadsheet (Schimmelpfennig et al., 2009) and the SLHL

460 production rate for spallation of Ca by Stone et al. (1996), which yields 14.4 ± 1.1 ka for
461 pyroxene and 14.3 ± 1.1 ka for plagioclase, confirming that pyroxene is a suitable mineral for
462 ^{36}Cl surface exposure age determinations.
463 Fig. 4 shows the ratios of the cosmogenic nuclide concentrations versus altitude. In pyroxene,
464 the mean values of the ratios and their standard deviations are 0.0582 ± 0.0061 (n=8) for
465 ^{36}Cl/^{3}He, 0.1864 ± 0.0085 (n=6) for ^{21}Ne/^{3}He and 0.301 ± 0.020 (n=6) for ^{36}Cl/^{21}Ne. For each of
466 the three TCN ratios, all individual measurements, except the ^{36}Cl/^{3}He ratio of TZ15, lie within
467 the standard deviation of the respective mean values and therefore do not show any altitudinal
468 dependence. It should be noted that TCN concentration ratios are composition-dependent,
469 particularly when ^{36}Cl and ^{21}Ne are involved, and they should not be expected to be the same in
470 different mineral phases or in pyroxenes with significantly different compositions. In this
471 study, the compositions of the pyroxene minerals are very similar, only TZ09 (En_{45}) and TZ15
472 (En_{44}) diverge slightly from the other samples (En_{41-43}). Significant differences are observed in
473 the Ca, Fe and Al concentrations (Table 2), each of them being an important target element
474 for at least one of the TCN in this study. Theoretical calculations of mineral production rates,
475 based on these compositions and on the elemental production rates by Masarik (2002), predict
476 that the ^{36}Cl/^{3}He and ^{36}Cl/^{21}Ne ratios of these two samples should be about 10% to 15% lower
477 than those of the other samples.
478 ^{21}Ne/^{3}He was also determined in olivine from four of the samples: TZ10 and TZ12 from the
479 2740 m sample site and TZ13 and TZ14 from the 3000 m site (Table 3b, Fig. 4b). At higher
480 altitudes, only ^{3}He could be determined in olivines. ^{36}Cl could not be measured in olivine since
481 this mineral contains no abundant target element for production of this nuclide. A mean
482 ^{21}Ne/^{3}He value of 0.377 ± 0.018 was determined and all four measurements lie within the
483 standard deviation of the mean value. No variation is observed between the two sample
484 locations.

485

486 - Fig. 4 about here -

487

488 ***4.2 Comparing apparent ^{36}Cl, ^{3}He and ^{21}Ne exposure ages***

489 If erosion is negligible, samples collected from a single lava-flow or glacially created surface
490 should yield the same exposure age irrespective of TCN or mineral phase. All composition-,
491 production pathway- and decay-related differences between the nuclides should be accounted
492 for in the exposure age calculation. Errors in scaling factors for spallation reactions will
493 cancel out provided the same scaling method is applicable for all reactions. A separate scaling
494 factor is required for production of ^{36}Cl from muons. However, errors in the muon scaling
495 factor are expected to have only a minor influence on calculated exposure age ratios, because
496 ^{36}Cl contributions from muons are not higher than 5-10%. We choose the scaling method of
497 Stone (2000), because all the SLHL production rates considered below were originally scaled
498 according to either Stone (2000) or to Lal (1991); these two methods are equivalent to each
499 other. The applied scaling factors are listed in Table 1.
500 The selection of SLHL production rates poses a more serious challenge, because for each
501 nuclide several experimentally calibrated and modelled production rates exist, covering a
502 quite large range of values. We will limit our study to select a single SLHL production rate for
503 each nuclide. If the SLHL production rates of all nuclides were perfectly known and all
504 nuclides were equally altitude-dependent, the exposure age ratios should be equal to 1 (cf. Fig.
505 5). Systematic discrepancies would indicate that one or both SLHL production rates are
506 inaccurate. Without an independent age control it is, however, not possible to determine
507 which production rate is correct.
508 For ^{36}Cl, production rates are not mineral- but target-element-specific. Spallation of Ca is the
509 most important production mechanism in our pyroxenes. We use the production rate for

510 spallation of Ca with a value of 48.8 ± 1.7 atoms (g Ca)$^{-1}$ a^{-1} (Stone et al., 1996). For ^{3}He, we
511 use the production rate of 128 ± 5 atoms (g mineral)$^{-1}$ a^{-1} (Blard et al., 2006). This production
512 rate is assumed to be valid for pyroxene as well as olivine because cosmogenic ^{3}He
513 concentrations are identical within analytical uncertainty in the cogenetic olivines and
514 pyroxenes of our study (Fig. 2). For ^{21}Ne, both modelled elemental production rates and
515 experimentally calibrated mineral-specific production rates are available. Here, we use the
516 calibrated SLHL production rate of 25 ± 8 atoms (g pyroxene)$^{-1}$ a^{-1} of Fenton et al. (2009). The
517 compositions of pyroxenes in Fenton et al. (2009) (En_{43-44}) fall within the range of those in our
518 study (En_{41-45}).
519 The resulting apparent exposure ages range between 14 ka and 170 ka (Table 4). For each
520 nuclide pair, the exposure age ratios are then calculated. These are plotted as a function of
521 altitude in Fig. 5. This graph shows a similar pattern to the concentration plot, indicating that
522 the radioactive decay of ^{36}Cl (as can be expected for relatively young exposure ages),
523 differences in mineral composition and the ^{36}Cl production by slow muon capture have only a
524 minor impact on the altitudinal trend of these data.
525 Despite this overall similarity, exposure age ratios appear to exhibit a slight dependence on
526 altitude. Notably ^{36}Cl/^{3}He decreases with altitude; this trend is essentially defined by samples
527 TZ09 (1000 m) and TZ15 (4100 m), with 30% difference between these two samples without
528 overlap of the estimated uncertainties. However, the TZ15 ^{36}Cl/^{21}Ne age ratio is
529 indistinguishable from those at lower altitudes. An error in the calculation of the ^{3}He age of
530 TZ15 is therefore possible. Since TZ15 was taken from a polished glacial surface of an old
531 dyke (see section 2, formation age >> exposure age), it is subject to an uncertain correction
532 for radiogenic ^{4}He*, which affects the cosmogenic ^{3}He concentration estimation (section 3.3).
533 The black circles at the altitude of TZ15 in Fig. 5a and b represent the age ratios when
534 assuming the highest correction for radiogenic ^{4}He* based on measured U and Th

535 concentrations, the $^{40}Ar/^{39}Ar$ age and the minimum grain size of the phenocrysts (2 mm). The
536 open circles mark the ratios if no such correction is done, thus indicating the trend towards
537 higher ratios if the radiogenic $^{4}He^{*}$ correction was overestimated. Furthermore, the surface of
538 the TZ09 flow was clearly eroded. Erosion can have an effect on ratios involving ^{36}Cl, because
539 it has a shorter half-life than the other nuclides and because the ^{36}Cl contribution from slow
540 negative-muon capture is less dependent on erosion than the ^{36}Cl contribution from spallation
541 due to the longer attenuation length of the muons. Consequently, if erosion is not taken into
542 account then the calculated apparent ^{36}Cl exposure age is higher relative to the calculated
543 apparent ^{3}He exposure age. The ratio of the apparent exposure ages of TZ09 is displayed in
544 Fig. 5a by the black circle, while the open diamond represents the ratio if erosion is taken into
545 account. For this calculation we assumed an eroded rock layer of 30 cm, which corresponds to
546 the estimated maximum erosion based on field evidence.
547 When these considerations are taken into account all exposure age ratios overlap within their
548 uncertainties over the examined altitude range. No clear altitudinal variation in nuclide
549 production can be demonstrated without ambiguity, regardless of the production rate or
550 nuclide pair examined. Also, no correlation of the ratios with the different exposure durations
551 of the surfaces can be observed.
552 At present, accurate independent age constraints are not available for the sampled lava flows,
553 preventing us from evaluating SLHL production rates. The production rates chosen here result
554 in exposure ages that mostly agree between all three nuclides (Table 4), i.e. the exposure age
555 ratios presented in Fig. 5 are generally equal to 1. But it is important to stress that this would
556 also have been the case if for all three nuclides accordingly lower or higher SLHL production
557 rates had been chosen and that this does not affect the evaluation of the altitude dependence of
558 the relative nuclide production rates.
559

- Table 4 -

- Fig. 5 about here -

5. Comparison with other cross-calibrations

A significant altitudinal variation of the relative production rates of ^{3}He compared to other nuclides, as was proposed by Gayer et al. (2004) and Amidon et al. (2008), is not documented by the Kilimanjaro data set. Even though the altitude range of samples TZ10 to TZ19 is similar to that of the Himalayan samples (3000 - 4600 m in Gayer et al., 2004, and 3200 - 4800 m in Amidon et al., 2008) and Amidon et al. (2008) documented an increase in the ^{3}He/^{10}Be concentration ratio of up to 40% for their transect, all exposure age ratios in our study agree at the 1σ level for the corresponding altitude range (2700 - 4300 m) (Fig. 5). Regarding only the nominal values of the ^{36}Cl/^{3}He exposure age ratios over the whole altitude range in our study (1000 – 4300 m), i.e. ignoring the overlapping uncertainties, results in a 17% increase. However, this variation is much less than that documented for the Himalayan transects (Fig. 6). Possible explanations could be that i) no significant differences in relative production rates exist and the anomaly in the nuclide ratios of the Himalayan samples is due to factors other than changes in the nucleon energy spectrum; ii) the altitude dependences of ^{36}Cl, ^{21}Ne and ^{3}He production are more similar than for ^{10}Be and ^{3}He; or iii) a latitude effect must be considered, since the Himalaya sites are at higher latitudes (27-28°N) than Mt. Kilimanjaro (3°S). Due to the decreasing shielding effect of the geomagnetic field with increasing latitude, the cosmic ray flux becomes stronger. As a consequence, the flux at 4000 m altitude and a latitude of 30° is about 35% higher than at the same altitude and a latitude of 3° (according to the scaling method by Stone, 2000). Also, at high latitudes the energy spectrum of the flux

585 becomes on average less energetic (Gosse and Phillips, 2001). This could explain different
586 altitude dependences of the relative production rates, even though the altitudes are very
587 similar for all studies considered here. However, the possibility of such a latitude effect has to
588 be further investigated.
589 The mean values of the $^{21}Ne/^{3}He$ concentration ratios in pyroxene (0.1864 ± 0.0085) and
590 olivine (0.377 ± 0.018) are slightly lower but in agreement within 1σ with those of a number
591 of studies undertaken at mid latitudes and altitudes between 1000 and 2000 m, e.g. Fenton et
592 al. (2009) (0.204 ± 0.014 in pyroxene and 0.400 ± 0.029 in olivine), Poreda and Cerling
593 (1992) (0.41 ± 0.05 in olivine) and Kounov et al. (2007) (0.225 ± 0.027 in pyroxene),
594 suggesting that the production rates of ^{3}He and ^{21}Ne in these minerals have the same altitude
595 and latitude dependences. However, two studies from Antarctica reported significantly higher
596 $^{21}Ne/^{3}He$ ratios in pyroxene from altitudes around 1000 – 2000 m (0.22-0.26 in Bruno et al.,
597 1997; 0.21 - 0.26 in Schäfer et al., 1999). The compositions of their pyroxenes are
598 significantly different from those in our study, but theoretical calculations based on these
599 compositions and the elemental production rates of Masarik (2002) predict $^{21}Ne/^{3}He$ ratios
600 lower than those in our study. The compositional differences cannot therefore explain the
601 discrepancy in the ratios. Other possible explanations are (i) the latitude effect proposed
602 before, suggesting that the production rate of ^{21}Ne increases at a higher rate than that of ^{3}He
603 with increasing latitude, or (ii) significant fractions of plagioclase and quartz in the Antarctic
604 pyroxene separates, as suggested by Niedermann et al. (2007). The presence of plagioclase
605 and quartz would lower the ^{3}He concentration, because these minerals are less retentive for
606 Helium than pyroxene. Several studies (Margerison et al., 2005, Niedermann et al., 2007,
607 Oberholzer et al., 2008) reported difficulties in obtaining pure pyroxene separates from the
608 sampled Antarctic dolerite, and $^{21}Ne/^{3}He$ ratios of four pure pyroxene separates re-measured

609 from the sample suite of Schäfer et al. (1999) are indeed lower (0.181-0.217, Niedermann et
610 al., 2007) than in the earlier study.
611 Staudacher and Allègre (1993) measured significantly lower $^{21}Ne/^{3}He$ ratios in olivine (0.23 -
612 0.30) at latitude 21°S and altitudes around 2300 m. Neither the mineral compositions, which
613 are very similar in their and our study, nor the hypothesized latitude effect seem likely to
614 explain this discrepancy. Assumedly, the calculations of their cosmogenic noble gas
615 concentrations were subject to inaccurate correction for non-cosmogenic components.
616 To our knowledge, Licciardi et al. (2008) is the only study in which ^{36}Cl has been co-calibrated
617 with another nuclide, ^{3}He. ^{36}Cl was measured in basaltic whole rock, while ^{3}He was determined
618 in olivine phenocrysts of the same samples (Licciardi et al., 2006). However, a comparison
619 between the relative production rates of ^{36}Cl and ^{3}He in their study and ours cannot be
620 performed for several reasons. ^{36}Cl concentrations are not given in Licciardi et al. (2008).
621 Also, the basalts have varying Cl concentrations (up to 61 ppm), which result in ^{36}Cl
622 contributions from capture of low-energy neutrons on ^{35}Cl of up to 26%, so that $^{36}Cl/^{3}He$
623 concentration ratios could not be expected to be constant from sample to sample. Finally, all
624 samples come from a narrow range of altitudes (20-460 m) excluding altitude dependent
625 comparisons.
626
627 - Fig. 6 about here -
628
629 **6. Conclusions**
630 This is the first study that deals with the cross-calibration of three cosmogenic nuclides (^{36}Cl,
631 ^{3}He and ^{21}Ne) in minerals over a large altitudinal profile (1000 - 4300 m) at low latitude (3° S).
632 All three nuclides have been measured in pyroxene phenocrysts, and ^{3}He and ^{21}Ne have
633 additionally been measured in olivine at two elevations. ^{36}Cl has also been determined in

plagioclase co-existing with pyroxene in one of the samples. Calculated exposure ages from both minerals yield the same result confirming the reliability of ^{36}Cl measurements in pyroxene.

Cosmogenic $^{21}Ne/^{3}He$ concentration ratios in pyroxene are 0.1864 ± 0.0085 and those in olivine are 0.377 ± 0.018, agreeing with previously determined ratios of these nuclides (Poreda and Cerling, 1992, Kounov et al., 2007, Fenton et al., 2009). In our samples, the $^{36}Cl/^{3}He$ and $^{36}Cl/^{21}Ne$ concentration ratios are 0.0582 ± 0.0061 and 0.301 ± 0.020, respectively. These concentration ratios can be very different between samples, since the ^{36}Cl production rate in a mineral depends strongly on the target element concentrations.

No significant altitude dependence of the relative production of any of the nuclides can be observed, in contrast to altitude-dependent variations documented in previous studies (Gayer et al., 2004, Amidon et al., 2008). Our observation is based on nuclide concentration ratios and calculated apparent exposure age ratios plotted versus the elevations of the sample sites. This suggests that production rates of the investigated nuclides are proportional to each other between mid and high altitudes at low latitude, implying that no nuclide-specific scaling factors are needed at this site. However, the latitude effect for cross-calibrations has to be further evaluated.

Although independently determined ages for the studied lava surfaces are not available at present, the consistency in the data-set should enable progress to be made in the determination of the production rates of all three nuclides as soon as the production rate of one of the nuclides has been accurately defined.

Acknowledgements:

F. Palhol and B. Marty are thanked for assistance in the field. This research would never have been possible without the enormous help from the University of Dar es Salaam, TANAPA, and Kilimanjaro National Park in Tanzania. We would particularly like to mention Dr. J. Wakibara (TANAPA), Fred Mangasini (University of Dar es Salaam) and Chamba Makene (Geological Survey of Tanzania), as well as Kilimanjaro guides R. Mtui and Zakaria and their team of porters at Marangu. Back in the laboratories, thanks goes to E. Davy for sample preparation, E. Schnabel for measurements at GFZ, B. Tibari and L. Zimmermann for help at CRPG, T. Guilderson and T. Brown as well as all the staff of the CAMS-LLNL for ^{36}Cl measurements and J. Wijbrans at Vrije Universiteit, Amsterdam, for $^{40}Ar/^{39}Ar$ analyses and discussion. Finally, David Shuster and an anonymous reviewer are gratefully acknowledged for their thorough and very constructive reviews that greatly improved the manuscript. This project was conducted as part of the CRONUS-EU Research Training Network (EU FP6 Marie Curie Actions, project 511927).

References:

Althaus, T., Niedermann, S., Erzinger, J., 2003. Noble gases in olivine phenocrysts from drill core samples of the Hawaii Scientific Drilling Project (HSDP) pilot and main holes (Mauna Loa and Mauna Kea, Hawaii). Geochemistry Geophysics Geosystems 4, 8701, doi: 10.1029/2001GC000275.

Amidon, W., Farley, K., Burbank, D., Prattsitaula, B., 2008. Anomalous cosmogenic ^{3}He production and elevation scaling in the high Himalaya. Earth and Planetary Science Letters 265 (1-2), 287-301.

683 Amidon, W. H., Rood, D. H., Farley, K. A., 2009. Cosmogenic ^{3}He and ^{21}Ne production rates calibrated against
684 ^{10}Be in minerals from the Coso volcanic field. Earth and Planetary Science Letters 280 (1-4), 194-204.
685
686 Balco, G., Shuster, D. L., 2009. Production rate of cosmogenic ^{21}Ne in quartz estimated from ^{10}Be, ^{26}Al, and ^{21}Ne
687 concentrations in slowly eroding Antarctic bedrock surfaces. Earth and Planetary Science Letters 281 (1-2), 48-
688 58.
689
690 Balco, G., Stone, J., Lifton, N., Dunai, T., 2008. A complete and easily accessible means of calculating surface
691 exposure ages or erosion rates from ^{10}Be and ^{26}Al measurements. Quaternary Geochronology 3 (3), 174-195.
692
693 Balco, G., Briner, J., Finkel, R. C., Rayburn, J. A., Ridge, J. C., Schaefer, J. M., 2009. Regional beryllium-10
694 production rate calibration for late-glacial northeastern North America. Quaternary Geochronology 4 (2), 93-107.
695
696 Blard, P. H., Farley, K. A., 2008. The influence of radiogenic ^{4}He on cosmogenic ^{3}He determinations in volcanic
697 olivine and pyroxene. Earth and Planetary Science Letters 276 (1-2), 20-29.
698
699 Blard, P. H., Pik, R., 2008. An alternative isochron method for measuring cosmogenic ^{3}He in lava flows.
700 Chemical Geology 251, 20-32.
701
702 Blard, P. H., Lavé, J., Pik, R., Quidelleur, X., Bourlés, D., Kieffer, G., 2005. Fossil cosmogenic ^{3}He record from
703 K-Ar dated basaltic flows of Mount Etna volcano (Sicily, 38°N): Evaluation of a new paleoaltimeter. Earth and
704 Planetary Science Letters 236, 613-631.
705
706 Blard, P. H., Pik, R., Lavé, J., Bourlès, D. L., Burnard, P., Yokochi, R., Marty, B., Trusdell, F., 2006.
707 Cosmogenic ^{3}He production rates revisited from evidences of grain size dependent release of matrix-sited helium.
708 Earth and Planetary Science Letters 247 (3-4), 222-234.
709
710 Bruno, L.A., Baur, H., Graf, T., Schlüchter, C., Signer, P., Wieler, R., 1997. Dating of Sirius Group Tillites in
711 the Antarctic Dry Valleys with cosmogenic ^{3}He and ^{21}Ne. Earth and Planetary Science Letters 147, 37–54.
712

713 Carignan, J., Hild, P., Mevelle, G., Morel, J., Yeghicheyan, D., 2001. Routine analyses of trace elements in
714 geological samples using flow injection and low pressure on-line liquid chromatography coupled to ICP-MS; a
715 study of geochemical reference materials BR, DR-N, UB-N, AN-G and GH. Geostandards Newsletter 25, 187-
716 198.
717
718 Cerling, T. E., Craig, H., 1994. Cosmogenic ^{3}He production rates from 39°N to 46°N latitude, western USA and
719 France. Geochimica et Cosmochimica Acta 58, 249-255.
720
721 Chmeleff, J., von Blanckenburg, F., Kossert, K., Jakob, D., 2010. Determination of the ^{10}Be half-life by
722 multicollector ICP-MS and liquid scintillation counting. Nuclear Instruments and Methods in Physics Research
723 Section B 268, 192-199.
724
725 Desilets, D., Zreda, M., 2003. Spatial and temporal distribution of secondary cosmic-ray nucleon intensities and
726 applications to in situ cosmogenic dating. Earth and Planetary Science Letters 206, 21-42.
727
728 Desilets, D., Zreda, M., Prabu, T., 2006. Extended scaling factors for in situ cosmogenic nuclides: New
729 measurements at low latitude. Earth and Planetary Science Letters 246 (3- 4), 265-276.
730
731 Downie, C., Wilkinson, P., 1972. The Geology of Kilimanjaro. The Department of Geology, The University of
732 Sheffield, Sheffield, 253 pp.
733
734 Dunai T. J., 2001a. Influence of secular variation of the geomagnetic field on production rates of in situ produced
735 cosmogenic nuclides. Earth and Planetary Science Letters 193, 197-212.
736
737 Dunai T.J, 2001b. Reply to comment on 'Scaling factors for production rates of in situ produced cosmogenic
738 nuclides: a critical reevaluation' by Darin Desilets, Marek Zreda and Nathaniel Lifton. Earth and Planetary
739 Science Letters 188, 289-298.
740
741 Dunai T.J., Wijbrans, J.R., 2000. Long-term cosmogenic ^{3}He production rates (152 ka-1.35 Ma) from ^{40}Ar/^{39}Ar
742 dated basalt flows at 29°N latitude. Earth and Planetary Science Letters 176, 147-156.

743

744 Dunai, T.J., Porcelli, D., 2002. Storage and transport of noble gases in the subcontinental lithosphere. Reviews in
745 Mineralogy and Geochemistry 47, 371-409.
746
747 Dunai, T. J., Stuart, F. M., Pik, R., Burnard, P., Gayer, E., 2007. Production of ^{3}He in crustal rocks by
748 cosmogenic thermal neutrons. Earth and Planetary Science Letters 258 (1-2), 228-236.
749
750 Eberhardt, P., Eugster, O., Marti, K., 1965. A redetermination of the isotopic composition of atmospheric neon.
751 Zeitschrift für Naturforschung 20a, 623-624.
752
753 Evans, J. M., Stone, J. O., Fifield, L. K., Cresswell, R. G., 1997. Cosmogenic ^{36}Cl production in K-feldspar.
754 Nuclear Instruments and Methods in Physics Research Section B 123, 334-340.
755
756 Farley, K. A., Libarkin, J., Mukhopadhyay, S., Amidon, W., 2006. Cosmogenic and nucleogenic ^{3}He in apatite,
757 titanite, and zircon. Earth and Planetary Science Letters 248 (1-2), 451-461.
758
759 Fenton, C. R., Niedermann, S., Goethals, M. M., Schneider, B., Wijbrans, J., 2009. Evaluation of cosmogenic
760 ^{3}He and ^{21}Ne production rates in olivine and pyroxene from two Pleistocene basalt flows, western Grand Canyon,
761 AZ, USA. Quaternary Geochronology 4, 475-492.
762
763 Gayer, E., Pik, R., Lavé, J., France-Lanord, C., Bourlès, D., Marty, B., 2004. Cosmogenic ^{3}He in Himalayan
764 garnets indicating an altitude dependence of the ^{3}He/^{10}Be production ratio. Earth and Planetary Science Letters
765 229 (1-2), 91-104.
766
767 Goethals, M. M., Hetzel, R., Niedermann, S., Wittmann, H., Fenton, C. R., Kubik, P. W., Christl, M., von
768 Blanckenburg, F., 2009. An improved experimental determination of cosmogenic ^{10}Be/^{21}Ne and ^{26}Al/^{21}Ne
769 production ratios in quartz. Earth and Planetary Science Letters 284, 187-198.
770
771 Gosse, J. C., Phillips, F. M., 2001. Terrestrial in situ cosmogenic nuclides: theory and application. Quaternary
772 Science Reviews 20, 1475-1560.

773

774 Kober, F., Ivy-Ochs, S., Leya, I., Baur, H., Magna, T., Wieler, R., Kubik, P. W., 2005. In situ cosmogenic ^{10}Be
775 and ^{21}Ne in sanidine and in situ cosmogenic ^{3}He in Fe-Ti-oxide minerals. Earth and Planetary Science Letters 236
776 (1-2), 404-418.
777
778 Korschinek, G., Bergmaier, A., Faestermann, T., Gerstmann, U. C., Knie, K., Rugel, G., Wallner, A., Dillmann,
779 I., Dollinger, G., Lierse von Gostomski, C., Kossert, K., Maiti, M., Poutivtsev, M., Remmert, A., 2010. A new
780 value for the half-life of ^{10}Be by Heavy-Ion Elastic Recoil Detection and liquid scintillation counting. Nuclear
781 Instruments and Methods in Physics Research Section B 268, 187-191.
782
783 Kounov, A., Niedermann, S., de Wit, M. J., Viola, G., Andreoli, M., Erzinger, J. (2007). Present denudation rates
784 at selected sections of the South African escarpment and the elevated continental interior based on cosmogenic
785 ^{3}He and ^{21}Ne. South African Journal of Geology 110, 235-248.
786
787 Kraml, M., Pik, R., Rahn, M., Carignan, J., Keller, J., 2006. A potential single grain ^{40}Ar/^{39}Ar, (U-Th)/He and FT
788 age standard: the Limberg t3 tuff. Geostandards and Geoanalytical Research 30, 73-86.
789
790 Kurz, M. D., 1986. In situ production of terrestrial cosmogenic helium and some applications to geochronology.
791 Geochimica et Cosmochimica Acta 50, 2855-2862.
792
793 Lal, D., 1991. Cosmic ray labeling of erosion surfaces: in situ nuclide production rates and erosion models. Earth
794 and Planetary Science Letters 104, 424-439.
795
796 Licciardi, J., Kurz, M., Curtice, J., 2006. Cosmogenic ^{3}He production rates from Holocene lava flows in Iceland.
797 Earth and Planetary Science Letters 246 (3-4), 251-264.
798
799 Licciardi, J., Denoncourt, C., Finkel, R., 2008. Cosmogenic ^{36}Cl production rates from Ca spallation in Iceland.
800 Earth and Planetary Science Letters 267 (1-2), 365-377.
801

802 Lifton, N., Bieber, J., Clem, J., Duldig, M., Evenson, P., Humble, J., Pyle, R., 2005. Addressing solar modulation
803 and long-term uncertainties in scaling secondary cosmic rays for in situ cosmogenic nuclide applications. Earth
804 and Planetary Science Letters 239, 140-161.
805
806 Margerison, H. R., Phillips, W. M., Stuart, F. M., Sugden, D. E., 2005. Cosmogenic ^{3}He concentrations in ancient
807 flood deposits from the Coombs Hills, northern Dry Valleys, East Antarctica: interpreting exposure ages and
808 erosion rates. Earth and Planetary Science Letters 230, 163-175.
809
810 Masarik, J., 2002. Numerical simulation of in-situ production of cosmogenic nuclides. Geochimica et
811 Cosmochimica Acta 66 (S1), Goldschmidt Conference Abstract A491.
812
813 Masarik, J., Reedy, R. C., 1996. Monte Carlo simulation of in-situ-produced cosmogenic nuclides. Radiocarbon
814 38, 163-164.
815
816 Niedermann, S., 2002. Cosmic-ray-produced noble gases in terrestrial rocks: Dating tools for surface processes.
817 Reviews in Mineralogy and Geochemistry 47, 731-784.
818
819 Niedermann, S., Goethals, M. M., Pilz, P., 2009. Evidence for a high ^{3}He or low ^{10}Be production rate from
820 cosmogenic nuclide cross-calibration. Geochimica et Cosmochimica Acta 73 (13, Suppl. 1), Goldschmidt
821 Conference Abstract A940.
822
823 Niedermann, S., Schaefer, J. M., Wieler, R., Naumann, R., 2007. The production rate of cosmogenic 38Ar from
824 calcium in terrestrial pyroxene. Earth and Planetary Science Letter 257, 596–608.
825
826 Nonnotte, P., Guillou, H., Gall, B. L., Benoit, M., Cotten, J., Scaillet, S., 2008. New K-Ar age determinations of
827 Kilimanjaro volcano in the North Tanzanian diverging rift, East Africa. Journal of Volcanology and Geothermal
828 Research 173 (1-2), 99-112.
829
830 Oberholzer, P., Baronik, C., Salvatore, M.C., Baur, H., Wieler, R., 2008. Dating late-Cenozoic erosional surfaces
831 in Victoria Land, Antarctica, with cosmogenic neon in pyroxene. Antarctic Science 20, 89-98.

Phillips, F. M., Plummer, M. A., 1996. CHLOE: A program for interpreting in-situ cosmogenic nuclide data for surface exposure dating and erosion studies. Abstracts of the 7th international conference on Accelerator Mass Spectrometry, 98-99.

Poreda, R. J., Cerling, T. E., 1992. Cosmogenic neon in recent lavas from the western United States. Geophysical Research Letters 19, 1863-1866.

Schäfer, J. M., Ivy-Ochs, S., Wieler, R., Leya, I., Baur, H., Denton, G. H., Schlüchter, C., 1999. Cosmogenic noble gas studies in the oldest landscape on earth: surface exposure ages of the Dry Valleys, Antarctica. Earth and Planetary Science Letters 167 (3-4), 215-226.

Schimmelpfennig, I., Benedetti, L., Finkel, R., Pik, R., Blard, P. H., Bourlès, D., Burnard, P., Williams, A., 2009. Sources of in-situ ^{36}Cl in basaltic rocks. Implications for calibration of production rates. Quaternary Geochronology 4, 441-461.

Schimmelpfennig, I., Benedetti, L., Garreta, V., Pik, R., Blard, P. H., Burnard, P., Bourlès, D., Finkel, R., Ammon, K., Dunai, T., 2011. Calibration of cosmogenic ^{36}Cl production rates from Ca and K spallation in lava flows from Mt. Etna (38°N, Italy) and Payun Matru (36°S, Argentina). Geochimica et Cosmochimica Acta 75, 2611-2632.

Shanahan, T. M., Zreda, M., 2000. Chronology of Quaternary glaciations in East Africa. Earth and Planetary Science Letters 177 (1-2), 23-42.

Sharma, P., Kubik, P. W., Fehn, U., Gove, H. E., Nishiizumi, K., Elmore, D., 1990. Development of ^{36}Cl standards for AMS. Nuclear Instruments and Methods in Physics Research Section B 52, 410-415.

Staudacher, T., Allègre, C.J., 1993. The cosmic ray produced ^{3}He/^{21}Ne ratio in ultramafic rocks. Geophysical Research Letters, 20, 1075-1078.

Stone, J. O., 2000. Air pressure and cosmogenic isotope production. Journal of Geophysical Research 105 (B10), 23753-23759.

Stone, J. O., Allan, G. L., Fifield, L. K., Cresswell, R. G., 1996. Cosmogenic ^{36}Cl from calcium spallation. Geochimica et Cosmochimica Acta 60 (4), 679-692.

Vermeesch, P., Baur, H., Heber, V. S., Kober, F., Oberholzer, P., Schaefer, J. M., Schlüchter, C., Strasky, S., Wieler, R., 2009. Cosmogenic ^{3}He and ^{21}Ne measured in quartz targets after one year of exposure in the Swiss Alps. Earth and Planetary Science Letters 284 (3-4), 417-425.

Table captions:

Table 1: Sample details. Geographic sample locations, scaling factors for neutron induced and slow negative muon induced reactions calculated according to Stone (2000), sample thickness and thickness correction factors for spallation reactions.

Table 2: Element concentrations in minerals. a) Concentrationsof target elements for ^{36}Cl production in pretreated pyroxene separates (px) and one plagioclase separate (plg) before ^{36}Cl extraction, determined by ICP-OES at the SARM (CRPG, France). "< D.L." = "below detection limit". b) Concentrations of U, Th and Li in chemically untreated pyroxene (px) and olivine (ol) separates, determined by ICP-MS (U, Th) and atomic absorption (Li) at SARM. c) Concentrations of target elements for ^{21}Ne production in chemically untreated pyroxene and olivine separates determined by electron microprobe at the Université Henri Poincaré on 6-8 grains (mean values and their standard deviations). Calculated elemental production rates for ^{21}Ne according to Masarik (2002) are also shown.

Table 3: Cosmogenic components of the measured ^{36}Cl, ^{3}He and ^{21}Ne concentrations and their ratios, with mean values and standard deviations, in a) pyroxene and b) olivine separates. Note that the ^{36}Cl concentrations of samples TZ10 and TZ12 are mean values of the two replicates of each (Table A1) with the corresponding standard deviations.

Table 4: Apparent exposure ages calculated using the cosmogenic ^{36}Cl, ^{3}He and ^{21}Ne concentrations in pyroxene (Table 3) and the SLHL production rates detailed in the footnotes. ^{36}Cl exposure ages were calculated with the ^{36}Cl calculation spreadsheet (Schimmelpfennig et al., 2009). Note that the ^{36}Cl exposure ages for samples TZ10 and TZ12 are mean values of the exposure ages of the two replicates of each with the corresponding standard deviations. The uncertainties (1σ) of the exposure ages do not include the uncertainties in the SLHL production rates, but those in the cosmogenic nuclide concentrations and for ^{36}Cl those in the contributions of the production reactions other than spallation.

Figure captions

Fig. 1: Sample location. a) Google Maps satellite image of Mt. Kilimanjaro, Tanzania. b) Side face (NW-SE) of Mt. Kilimanjaro (Image PIA03355, Courtesy NASA/JPL-Caltech), showing its peaks Shira, Kibo and Mawenzi as well as the sample locations and altitudes. Topography is vertically exaggerated two times.

Fig. 2: Cosmogenic ^{3}He concentrations in olivine and pyroxene phenocrysts. The red lines represent the mean values of the concentrations in pyroxene. For sample TZ09 ^{3}He was only measured in pyroxene.

Fig. 3: Neon three-isotope diagram showing data from olivines and pyroxenes at two temperature steps. The regression line defines a spallation line, which passes through the air component and is indistinguishable from the air-spallation mixing line of Schäfer et al. (1999).

Fig. 4: TCN ratios, calculated from the total cosmogenic ^{3}He, ^{21}Ne and ^{36}Cl concentrations, as a function of altitude. Black circles correspond to the ratios in pyroxene, gray circles to those in olivine. The continuous and dashed lines indicate the means of the ratios and their standard deviations, respectively, with values given to the left.

Fig. 5: Exposure age ratios calculated from cosmogenic ^{36}Cl, ^{3}He and ^{21}Ne concentrations in pyroxene. Production rates used are: 48.8 atoms (g Ca)$^{-1}$ a^{-1} for ^{36}Cl (Stone et al., 1996), 128 atoms (g mineral)$^{-1}$ a^{-1} for ^{3}He (Blard et al., 2006) and 25 atoms (g mineral)$^{-1}$ a^{-1} for ^{21}Ne (Fenton et al., 2009). Standard deviations of these production rates are not propagated in the ratio uncertainties (see Table 4). The black circles at the altitude of sample TZ15 in panels a) and b) represent the age ratios when assuming the highest possible correction for radiogenic ^{4}He*, while the open circles mark the ratios if no such correction is done (see text for details). The black circle at the altitude of TZ09 in panel a) represents the age ratio ignoring erosion, while the open diamond represents the ratio if erosion is taken into account (see text for details).

Fig. 6: ^{36}Cl/^{3}He exposure age ratios as in Fig. 5a with apparent altitudinal trend. TZ15 is not considered due to uncertain cosmogenic ^{3}He concentrations, and the TZ09 composition has been corrected for erosion (section 4.2). The 40% increase of the ^{3}He/^{10}Be trend in Himalayan zircons between 3200 and 4800 m

(Amidon et al., 2008) is indicated in gray. Note that here ^{10}Be/^{3}He concentration ratios are compared to ^{36}Cl/^{3}He exposure age ratios.

Figure 1

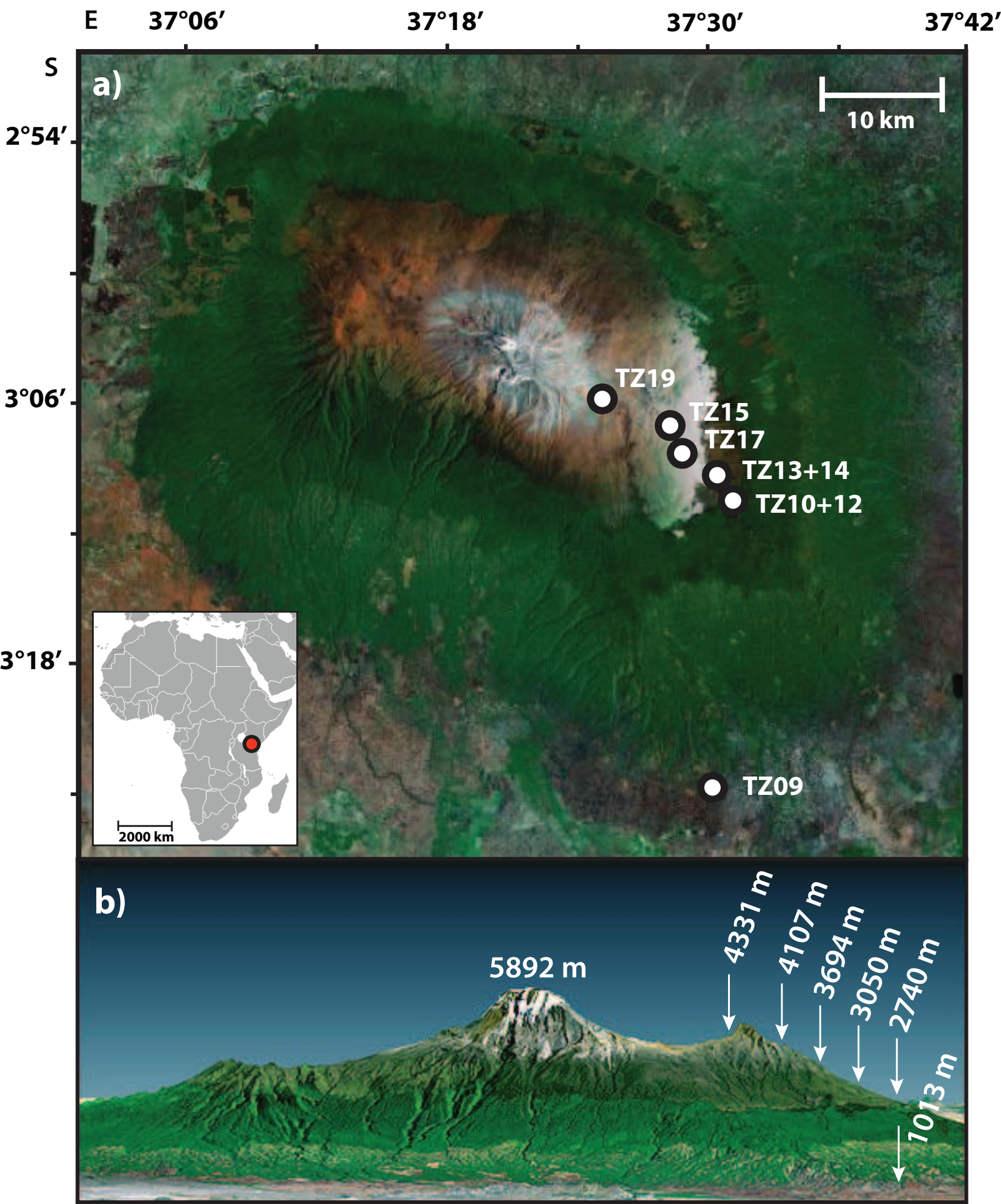
E
37°06′
37°18′
37°30′
37°42′
S
2°54′
3°06′
3°18′
a)
10 km
TZ19
TZ15
TZ17
TZ13+14
TZ10+12
TZ09
2000 km
b)
5892 m
4331 m
4107 m
3694 m
3050 m
2740 m
1013 m

Figure 2

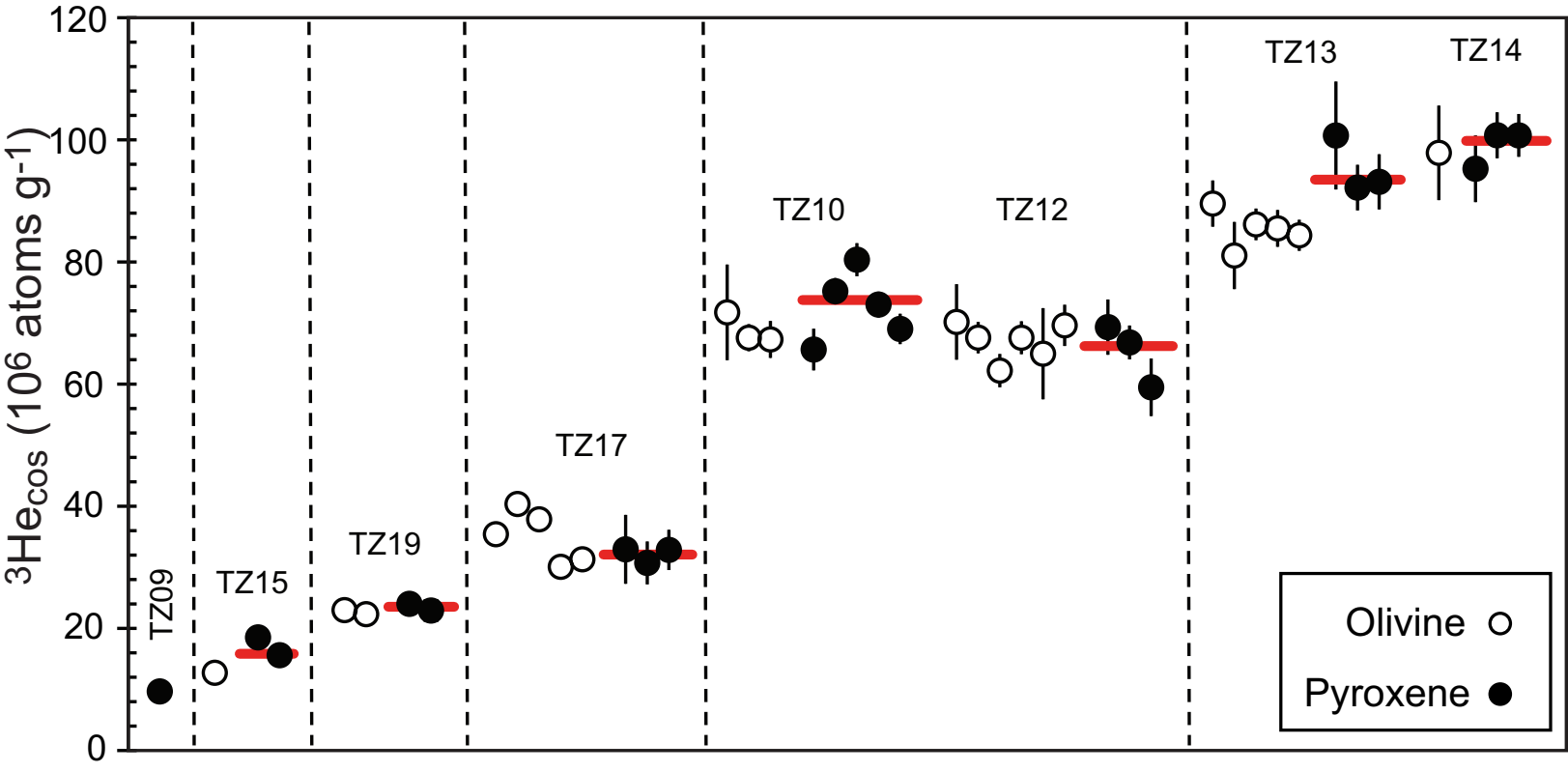
120
100
80
60
40
20
0
$^3He_{cos}$ (10^6 atoms g^{-1})
TZ09
TZ15
TZ19
TZ17
TZ10
TZ12
TZ13
TZ14
Olivine
Pyroxene

Figure 3

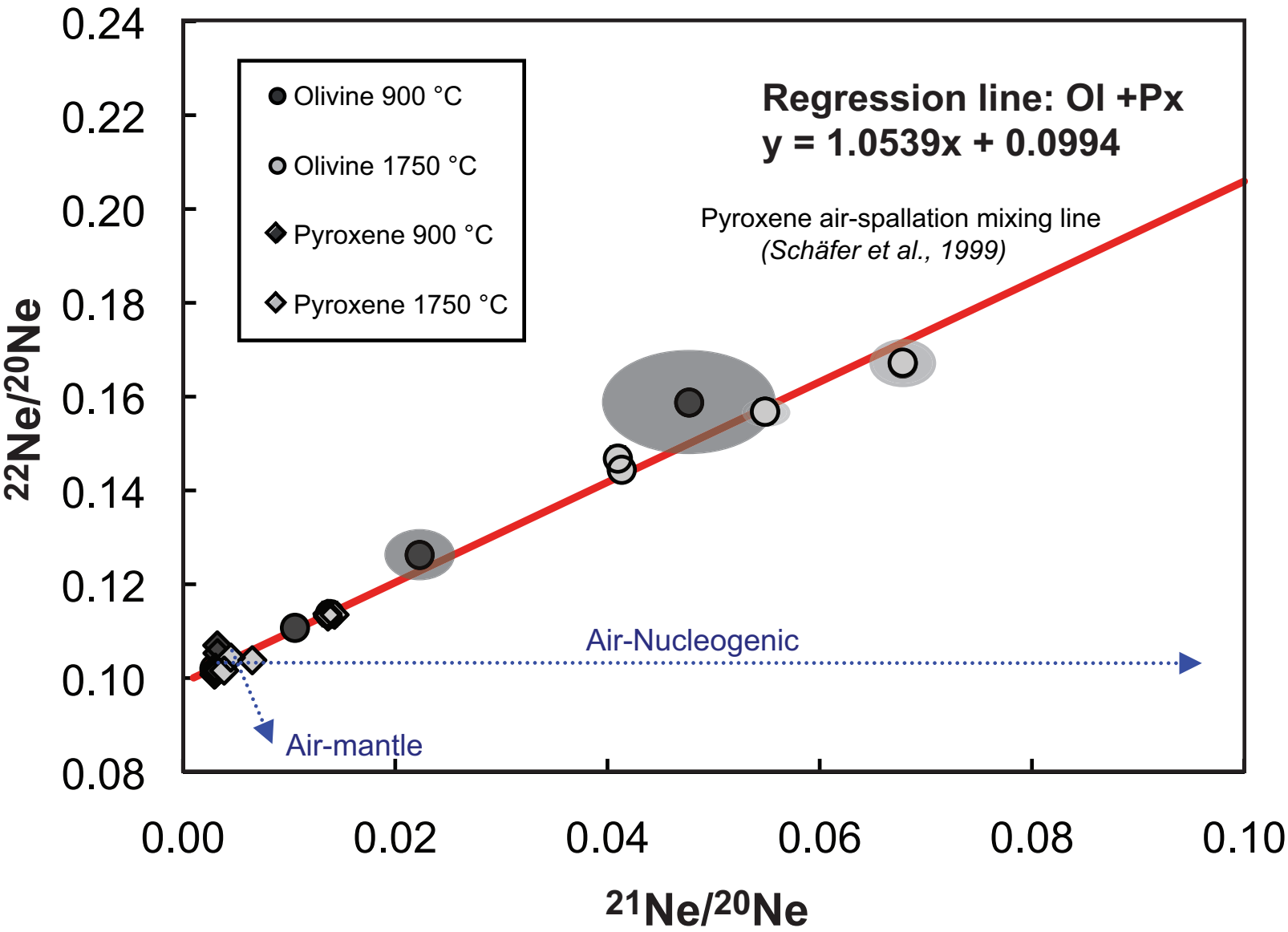
Olivine 900 °C
Olivine 1750 °C
Pyroxene 900 °C
Pyroxene 1750 °C
Regression line: Ol +Px
y = 1.0539x + 0.0994
Pyroxene air-spallation mixing line
(Schäfer et al., 1999)
Air-Nucleogenic
Air-mantle
0.24
0.22
0.20
0.18
0.16
0.14
0.12
0.10
0.08
0.00
0.02
0.04
0.06
0.08
0.10
22Ne/20Ne
21Ne/20Ne

Figure 4

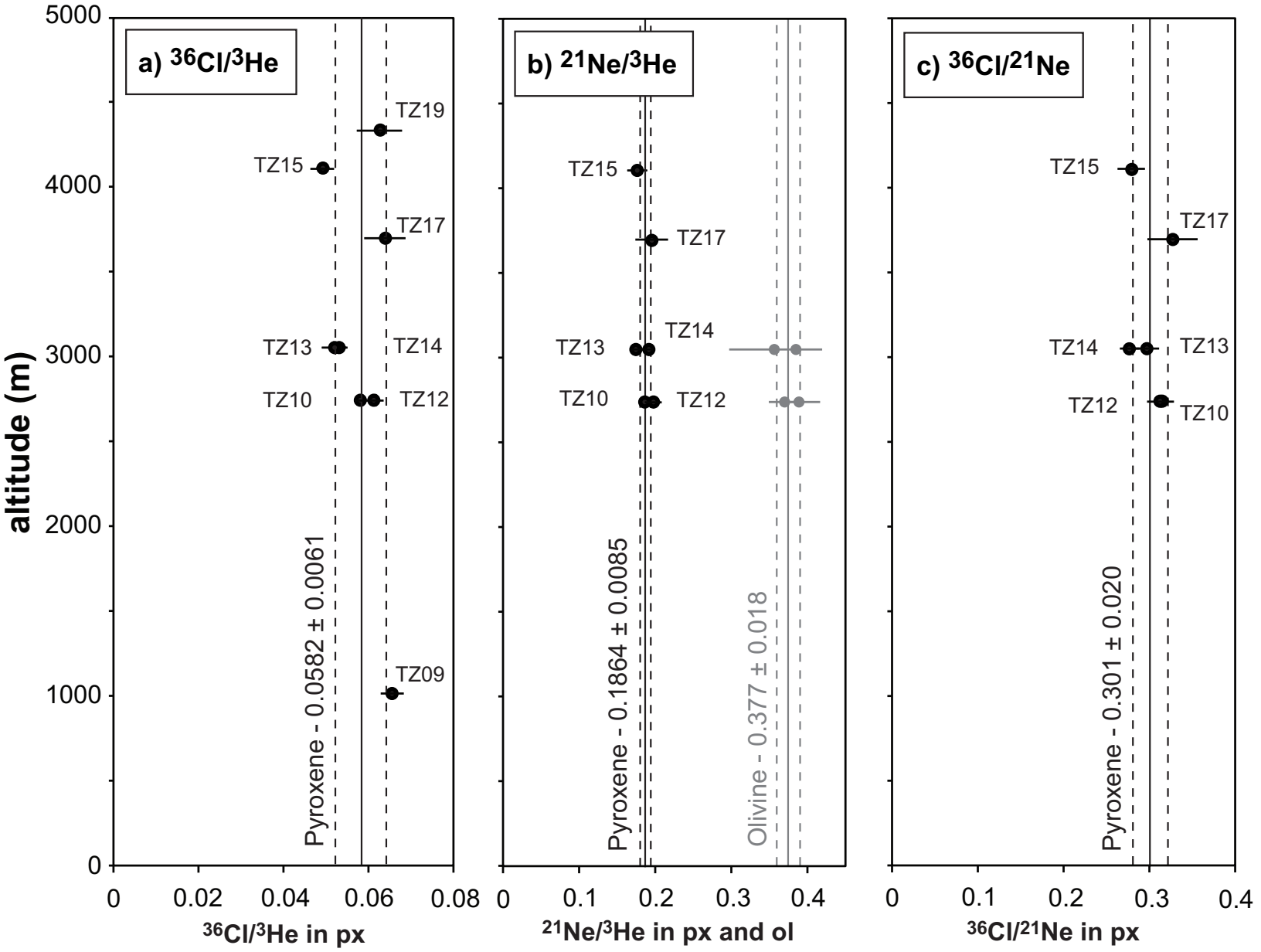
a) 36Cl/3He
b) 21Ne/3He
c) 36Cl/21Ne
altitude (m)
5000
4000
3000
2000
1000
0
TZ19
TZ15
TZ17
TZ13
TZ14
TZ10
TZ12
TZ09
Pyroxene - 0.0582 ± 0.0061
Pyroxene - 0.1864 ± 0.0085
Olivine - 0.377 ± 0.018
Pyroxene - 0.301 ± 0.020
0
0.02
0.04
0.06
0.08
0.1
0.2
0.3
0.4
36Cl/3He in px
21Ne/3He in px and ol
36Cl/21Ne in px

Figure 5

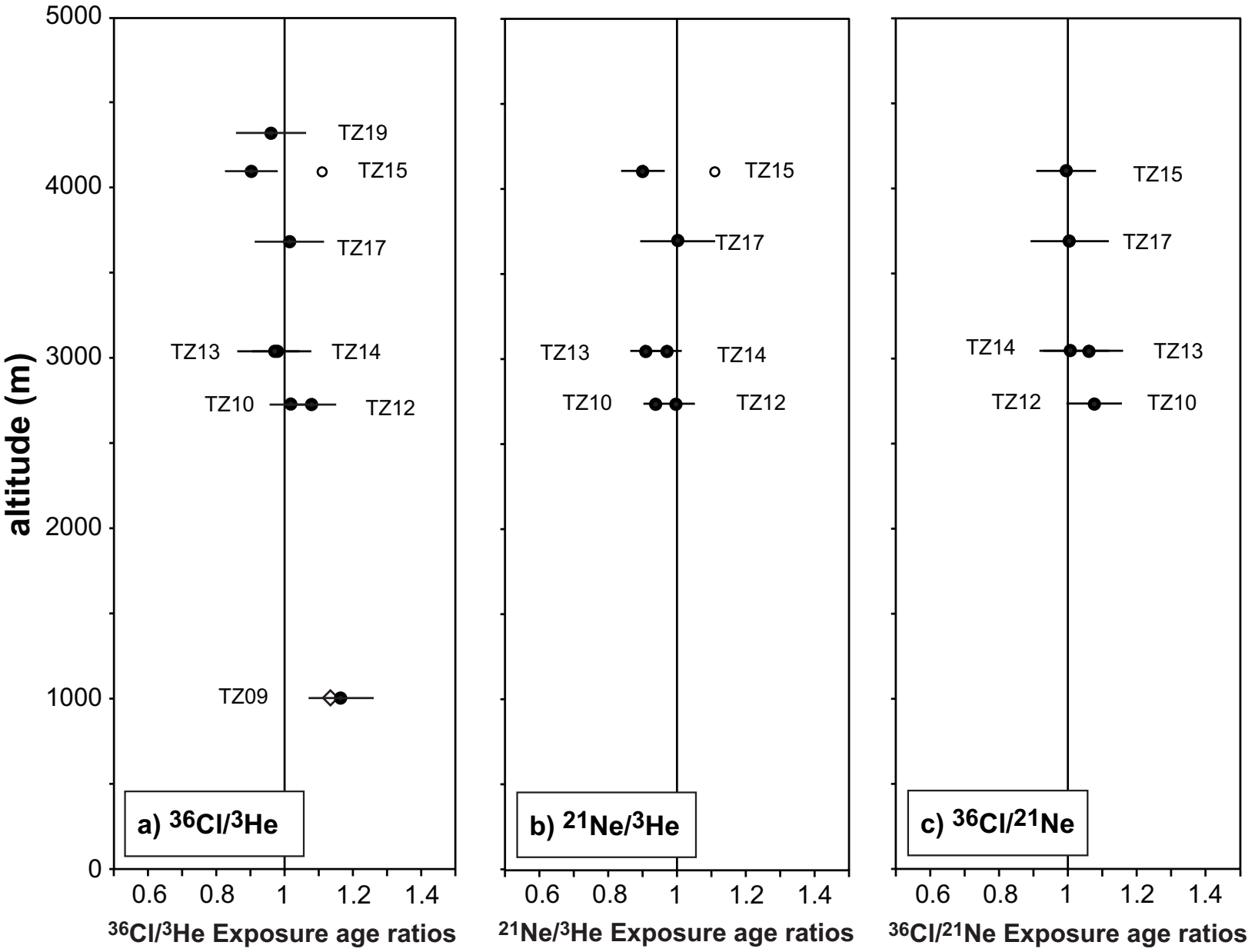
altitude (m)
5000
4000
3000
2000
1000
0
TZ19
TZ15
TZ17
TZ13
TZ14
TZ10
TZ12
TZ09
a) 36Cl/3He
0.6
0.8
1
1.2
1.4
36Cl/3He Exposure age ratios
TZ15
TZ17
TZ13
TZ14
TZ10
TZ12
b) 21Ne/3He
21Ne/3He Exposure age ratios
TZ15
TZ17
TZ14
TZ13
TZ12
TZ10
c) 36Cl/21Ne
36Cl/21Ne Exposure age ratios

Figure 6

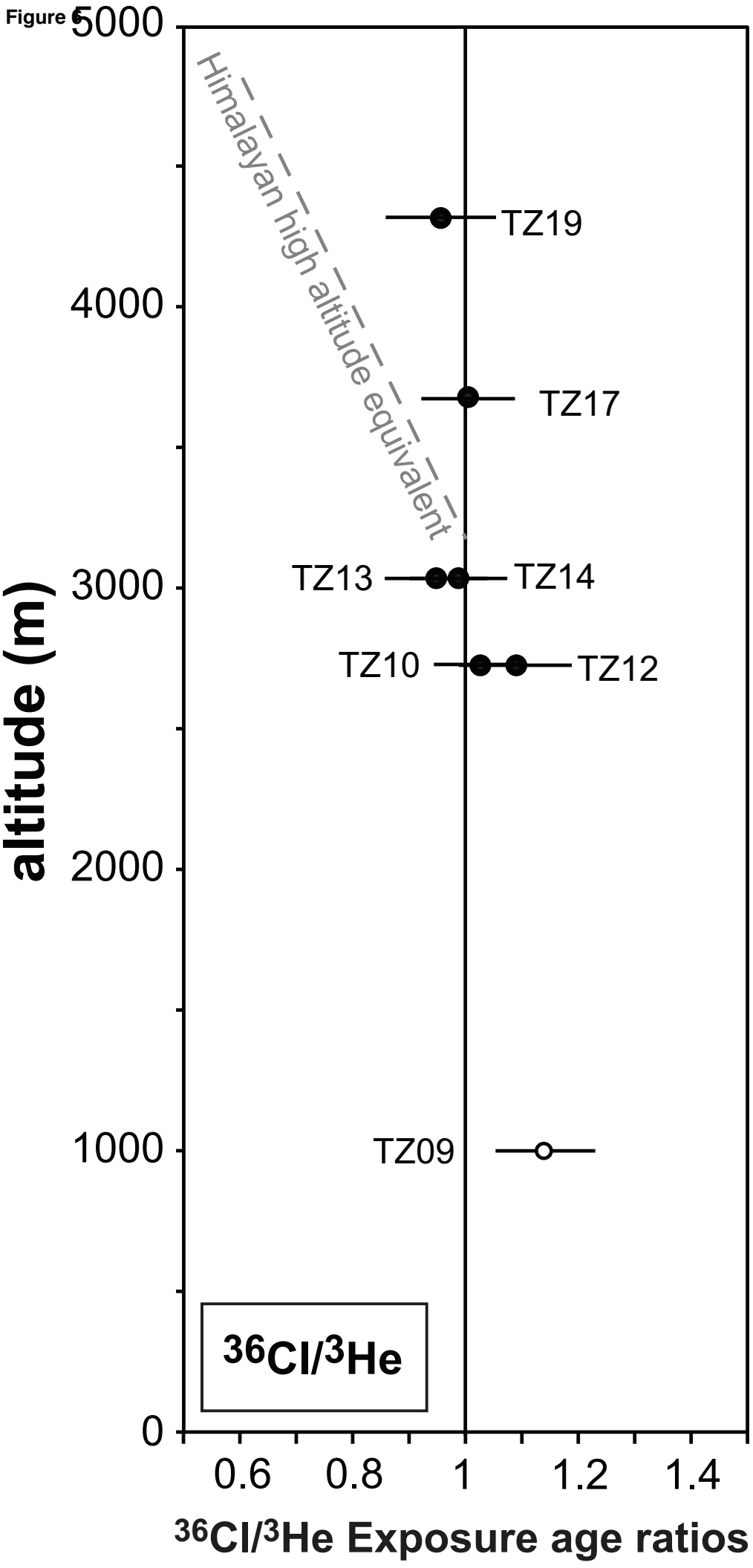
5000
4000
3000
2000
1000
0
altitude (m)
Himalayan high altitude equivalent
TZ19
TZ17
TZ13
TZ14
TZ10
TZ12
TZ09
36Cl/3He
0.6
0.8
1
1.2
1.4
36Cl/3He Exposure age ratios

Table 1

Sample	latitude South	longitude East	altitude [m]	scaling neutrons	scaling muons	thickness [cm]	thickness correction
TZ09	03° 23′.740	37° 30′.248	1013	1.27	0.95	5.3	0.957
TZ10	03° 10′.490	37° 31′.180	2740	3.94	1.95	5.8	0.953
TZ12	03° 10′.490	37° 31′.180	2740	3.94	1.95	5.7	0.953
TZ13	03° 09′.319	37° 30′.411	3050	4.69	2.19	4.5	0.963
TZ14	03° 09′.319	37° 30′.411	3050	4.69	2.19	5.1	0.958
TZ17	03° 08′.308	37° 28′.791	3694	6.56	2.75	6.8	0.945
TZ15	03° 07′.020	37° 28′.234	4107	8.02	3.16	4.2	0.965
TZ19	03° 05′.791	37° 25′.240	4331	8.90	3.39	7.2	0.942

Table 2

a)

Sample	Ca [%]	K [%]	Ti [%]	Fe [%]
TZ09-px	13.87± 0.28	< D.L.	0.88± 0.04	5.71± 0.11
TZ10A-px	15.71± 0.31	< D.L.	1.37± 0.07	4.66± 0.09
TZ10B-px	15.69± 0.31	< D.L.	1.38± 0.07	4.68± 0.09
TZ12A-px	15.56± 0.31	< D.L.	1.37± 0.07	4.65± 0.09
TZ12B-px	15.48± 0.31	< D.L.	1.33± 0.07	4.77± 0.10
TZ13-px	15.19± 0.30	< D.L.	1.16± 0.06	4.64± 0.09
TZ14-px	15.14± 0.30	< D.L.	1.11± 0.05	4.58± 0.09
TZ17-px	15.22± 0.31	0.04± 0.01	1.16± 0.06	4.57± 0.09
TZ15-px	13.06± 0.26	< D.L.	0.98± 0.05	7.61± 0.15
TZ19-px	15.44± 0.31	< D.L.	1.49± 0.07	5.32± 0.10
TZ15-plg	7.46± 0.15	0.50± 0.02	0.10± 0.01	0.45± 0.01

b)

Sample	U [ppm]	Th [ppm]	Li [ppm]
TZ09-px	0.039	0.156	3.2
TZ12-px	0.079	0.443	2.9
TZ14-px	0.113	0.455	2.3
TZ17-px	0.100	0.460	-
TZ15-px	0.086	0.282	4.5
TZ19-px	0.123	0.546	7.0
TZ12-ol	0.042	0.059	-
TZ14-ol	0.038	0.062	2.4
TZ17-ol	0.068	0.030	2.0
TZ15-ol	0.086	0.165	6.8
TZ19-ol	0.035	0.038	2.4

c)

Sample	Mg [%]	Al [%]	Si [%]	Ca [%]	Fe [%]	Na [%]
TZ10/12-px	8.06±0.43	3.70±0.30	22.24±0.52	16.23±0.22	4.60±0.40	0.55±0.04
TZ13/14-px	8.85±0.58	3.03±0.50	23.23±0.62	15.73±0.34	4.20±0.48	0.56±0.02
TZ17-px	10.04±0.24	1.97±0.26	24.32±0.25	15.34±0.21	3.33±0.13	0.51±0.03
TZ15-px	9.17±0.68	1.65±0.24	23.92±0.46	14.45±0.54	7.03±1.47	0.35±0.03
TZ10/12-ol	26.13±0.64	0.01±0.03	18.76±0.24	0.39±0.30	12.96±1.03	0.02±0.03
TZ13/14-ol	25.79±0.73	0.01±0.03	18.64±0.17	0.26±0.14	13.46±1.06	0.02±0.02
elemental prod. rates[a]	175.1	62.4	41.7	1.8	0.2	102.0

[a] [atoms ^{21}Ne (g element)$^{-1}$ a^{-1}]

Table 3

a) Pyroxene

Sample	$[^{36}Cl]$ (px) $[10^6$ atoms $g^{-1}]$	$[^3He]_{cos}$ (px) $[10^6$ atoms $g^{-1}]$	$[^{21}Ne]_{cos}$ (px) $[10^6$ atoms $g^{-1}]$	$[^{36}Cl]/[^3He]$ (px)	$[^{21}Ne]/[^3He]$ (px)	$[^{36}Cl]/[^{21}Ne]$ (px)
TZ09	0.631 ± 0.017	9.60 ± 0.29		0.0658 ± 0.0027		
TZ10	4.246 ± 0.065	73.8 ± 1.1	13.52 ± 0.44	0.0576 ± 0.0012	0.1834 ± 0.0066	0.314 ± 0.011
TZ12	4.029 ± 0.074	66.2 ± 2.1	12.91 ± 0.60	0.0608 ± 0.0022	0.195 ± 0.011	0.312 ± 0.016
TZ13	4.94 ± 0.12	93.5 ± 2.7	16.62 ± 0.67	0.0529 ± 0.0020	0.1780 ± 0.0089	0.297 ± 0.014
TZ14	5.25 ± 0.10	99.8 ± 2.3	18.96 ± 0.69	0.0526 ± 0.0016	0.1899 ± 0.0082	0.277 ± 0.011
TZ17	2.059 ± 0.059	32.1 ± 2.2[a]	6.30 ± 0.53	0.0642 ± 0.0048	0.196 ± 0.021	0.327 ± 0.029
TZ15	0.781 ± 0.021	15.84 ± 0.78	2.79 ± 0.14	0.0493 ± 0.0028	0.176 ± 0.012	0.279 ± 0.016
TZ19	1.47 ± 0.10	23.5 ± 1.1[a]		0.0626 ± 0.0052		
mean ± st.dev				0.0582 ± 0.0061	0.1864 ± 0.0085	0.301 ± 0.020

b) Olivine

Sample	$[^3He]_{cos}$ (ol) $[10^6$ atoms $g^{-1}]$	$[^{21}Ne]_{cos}$ (ol) $[10^6$ atoms $g^{-1}]$	$[^{21}Ne]/[^3He]$ (ol)
TZ10	67.7 ± 1.8	26.8 ± 1.4	0.396 ± 0.023
TZ12	66.9 ± 1.4	24.8 ± 1.2	0.371 ± 0.019
TZ13	85.7 ± 1.4	32.8 ± 1.4	0.383 ± 0.017
TZ14	97.9 ± 7.7	34.9 ± 2.2	0.357 ± 0.061
TZ17	34.88 ± 0.54		
TZ15	13.13 ± 0.59		
TZ19	22.84 ± 0.52		
mean ± st.dev			0.377 ± 0.018

[a] Magmatic $^3He/^4He$ values were determined applying the isochron method by Blard and Pik (2008)

Table 4

Sample	^{36}Cl (px) [a] [ka]	^{3}He (px) [b] [ka]	^{21}Ne (px) [c] [ka]
TZ09	71.7± 5.4	61.7± 1.9	
TZ10	156.1± 9.1	154± 2.3	144.3± 4.7
TZ12	148.7± 8.7	137.9± 4.4	137.6± 6.4
TZ13	157± 13	161.9± 4.7	147.5± 5.9
TZ14	171± 14	173.7± 4.0	168.9± 6.1
TZ17	40.9± 3.0	40.4± 2.8	40.6 ± 3.4
TZ15	14.4± 1.0	15.98± 0.78	14.43± 0.72
TZ19	21.1± 2.0	21.90± 1.0	

[a] ^{36}Cl SLHL production for spallation of Ca 48.8±1.7 atoms ^{36}Cl (g Ca)$^{-1}$ a^{-1} according to Stone et al. (1996)
[b] ^{3}He SLHL production for pyroxene 128±5 atoms ^{3}He (g px)$^{-1}$ a^{-1} according to Blard et al. (2006)
[c] ^{21}Ne SLHL production for pyroxene 25±8 atoms ^{21}Ne (g px)$^{-1}$ a^{-1} according to Fenton et al. (2009)

Supplementary Data

Click here to download Supplementary Data: Supplementary_Material.pdf